# Varicella-Zoster Virus ORF9 Is an Antagonist of the DNA Sensor cGAS

Jonny Hertzog[1], Rachel E. Rigby[1], Sonja Roll[1], Chiara Cursi[1], Lise Chauveau[1], Tamara Davenne[1], and Jan Rehwinkel[1,*]

[1]MRC Human Immunology Unit, MRC Weatherall Institute of Molecular Medicine, Radcliffe Department of Medicine, University of Oxford, Oxford, UK

*correspondence: jan.rehwinkel@imm.ox.ac.uk

## ABSTRACT

Varicella-Zoster virus (VZV) causes chickenpox and shingles. Although infection is associated with severe morbidity in some individuals, the molecular mechanisms that determine innate immune responses remain poorly defined. We found that the cGAS/STING DNA sensing pathway was critically required for type I interferon (IFN) induction in response to VZV infection. Viral gene overexpression screening identified the essential VZV tegument protein ORF9 as a novel antagonist of DNA sensing via cGAS. Ectopically as well as virally expressed ORF9 bound to endogenous cGAS. Confocal microscopy revealed co-localisation of cGAS and ORF9, which blocked the type I IFN response to transfected DNA. ORF9 and cGAS also interacted directly in a cell-free system. Our data further suggest that ORF9 inhibited the production of cGAMP by cGAS. Taken together, our work highlights the importance of the cGAS/STING DNA sensing pathway for VZV recognition and identified an immune antagonist encoded by VZV that directly interferes with DNA sensing *via* cGAS.

## INTRODUCTION

Varicella-Zoster virus (VZV) is one of nine herpes viruses that infect humans (Arvin and Gilden, 2013). VZV is an alpha-herpesvirus, closely related to Herpes Simplex virus (HSV) 1 and 2. It has a 125kb dsDNA genome, the smallest of the human herpesviruses. The genome includes at least 70 open reading frames (ORFs). Primary infection causes chickenpox (*Varicella*). Like all human herpes viruses, VZV establishes life-long latency in an infected host and can reactivate as shingles (*Zoster*). Shingles is a debilitating disease with significant associated morbidity. During both primary infection and reactivation, the virus can gain access to the central nervous system and cause severe complications such as encephalitis and vasculitis (Nagel and Gilden, 2014). Despite introduction of the live-attenuated chickenpox vaccine in the early 1990s, the virus remains highly prevalent worldwide (WHO, 2014).

The type I IFN system lies at the forefront of host defence against infectious pathogens and is indispensable for successful control of viral infections (McNab et al., 2015). The expression of these cytokines is induced following pattern recognition receptor (PRR) activation. PRRs are a heterogenous group of proteins that can respond to a diverse array of pathogen-associated molecular patterns (PAMPs) (Brubaker et al., 2015). The recognition of viral pathogens relies to a large extent on sensing of nucleic acids (Barrat et al., 2016; Hartmann, 2017). Both endosomal toll-like receptors and dedicated cytosolic sensors are potently activated by viral RNA and DNA. The DNA sensor cyclic GMP-AMP synthase (cGAS) synthesises the second messenger 2'3'-cyclic GMP-AMP (hereafter simply cGAMP), a cyclic di-nucleotide, upon direct binding to dsDNA (Ablasser et al., 2013; Sun et al., 2013; Wu et al., 2013). Binding of cGAMP to stimulator of IFN genes (STING) results in the activation of the transcription factors IRF3 and NFκB via the kinases TBK1 and IKKε (de Oliveira Mann et al., 2019; Diner et al., 2013; Fitzgerald et al., 2003; Ishikawa et al., 2009; Liu et al., 2015; Sharma et al., 2003; Zhang et al., 2019; Zhang et al., 2013) . Both transcription factors are responsible for the expression of IFNβ and other type I and type III IFNs, as well as inflammatory cytokines. Other proteins, such as IFI16, RNA polymerase III, and DNA-PK have been described to be accessory proteins to the cGAS/STING system or constitute independent DNA-sensing mechanisms (Dempsey and Bowie, 2015).

Type I IFNs are secreted cytokines that act in an autocrine, paracrine, or systemic manner by binding to the type I IFN receptor (IFNAR) (McNab et al., 2015). Canonical IFNAR signalling results in the phosphorylation and heterodimerisation of the transcription factors STAT1 and STAT2. After recruitment of IRF9, this protein complex drives expression of hundreds of genes, termed interferon-stimulated genes (ISGs). Among others, ISGs contain genes that encode PRRs, proteins involved in type I IFN induction and signalling, negative and positive feedback regulators, restriction factors acting directly on viruses, and proteins that are involved in adaptive immune responses (Schoggins, 2019; Schoggins et al., 2011).

Despite the fact that VZV is a highly prevalent and important human pathogen, its pathogenesis is still poorly understood. The lack of suitable small animal models that recapitulate primary infection and latency establishment has hampered the molecular

73 characterisation of its life cycle *in vivo* (Haberthur and Messaoudi, 2013). During its
74 dissemination in the human host, the virus infects a multitude of different cells. Infection
75 of T cells, keratinocytes, neurons, and epithelial cells is indispensable for VZV's life
76 cycle (Zerboni et al., 2014). In addition, immune cells including dendritic cells (DCs),
77 monocytes, and NK cells are capable of supporting VZV replication *in vitro* and are
78 potentially relevant for *in vivo* spread (Abendroth et al., 2001; Campbell et al., 2018;
79 Kennedy et al., 2019; Morrow et al., 2003; Wang et al., 2005). However, the events that
80 govern the cell-intrinsic recognition of the virus in these cell types and the antiviral
81 cytokine response have only begun to be elucidated *in vitro*. The DNA sensor TLR9 is
82 partly responsible for IFNα secretion after infection of plasmacytoid DCs (Yu et al.,
83 2011). In dermal fibroblasts, STING is required for type I and type III IFN production
84 (Kim et al., 2017). An interesting genetic link between DNA sensing *via* RNA polymerase
85 III and VZV CNS infection has been uncovered recently (Carter-Timofte et al., 2018).
86 Although a comprehensive characterisation of the role of these DNA sensing pathways
87 during VZV infection is lacking, current evidence suggests that type I IFNs are of critical
88 relevance for control of VZV infection. Increased IFNα levels can be detected in the
89 serum of patients with primary VZV infection (Arvin et al., 1986). In addition, the potency
90 of type I IFNs in restriction of VZV replication has been demonstrated *in vitro* (Kim et
91 al., 2017; Ku et al., 2016; Shakya et al., 2019; Torigo et al., 2000).
92 In this study we addressed the question which nucleic acid sensors induce type I IFN
93 expression in response to VZV infection. We show that the cGAS - STING - TBK1 -
94 IRF3 signalling axis was responsible for antiviral cytokine expression after VZV
95 infection. We further report the generation of a VZV ORF expression library and
96 identification of a viral cGAS antagonist. The tegument protein encoded by ORF9
97 blocked activation of cGAS and subsequent synthesis of cGAMP. Mechanistically, we
98 show that ORF9 interacted with cGAS, likely by binding to DNA. We propose a model
99 in which cGAS activation upon VZV infection is prevented immediately after viral entry
100 through the tegument protein ORF9.
101

102 # RESULTS
103
104 ## A Model System for VZV Infection
105 To identify PRRs that induce type I IFN in response to VZV infection we chose to use
106 the monocytic cell line THP1. We hypothesised a role of DNA sensors in VZV infection
107 given its identity as a DNA virus and the previously shown role of STING in recognition
108 of VZV (Kim et al., 2017). THP1 cells, unlike many other immortalised cell lines, induce
109 type I and type III IFNs *via* cGAS in response to DNA (Sun et al., 2013; Wu et al., 2013).
110 Furthermore, THP1 cells are amenable to genome editing and knockout (KO) lines can
111 be used to genetically dissect the role of individual proteins involved in pattern
112 recognition. THP1 cells are permissive for VZV infection and propagation (Nour et al.,
113 2011) and VZV infects primary human monocytes and macrophages *in vitro* and *in vivo*
114 (Kennedy et al., 2019; Mainka et al., 1998). In addition to wild-type (WT) THP1 cells, we
115 tested previously described KO lines lacking cGAS, STING, TBK1, MyD88, or IFNAR2.
116 We further generated MAVS KO and IRF3 KO cells using CRISPR/Cas9 technology
117 (see Materials and Methods and Figure S1). All THP1 KO cells were validated by
118 immunoblotting for the absence of protein and functionally by stimulation with DNA,
119 RNA and type I IFN (Figure S2).
120 Upon treatment with PMA, THP1 cells adopt a macrophage-like, adherent and highly
121 responsive phenotype. Given the difficulties of working with cell-free VZV (Caunt and
122 Taylor-Robinson, 2009; Chen et al., 2004), we used co-culture with VZV-infected (+VZV)
123 MeWo cells to infect PMA-treated THP1 cells; co-culture with uninfected MeWo cells
124 served as a control (Figure S3A). MeWo cells are a melanoma cell line that is well-
125 established for VZV propagation. After 48 hours of co-culture, cells were harvested for
126 RT-qPCR, immunoblotting, and flow cytometry analysis. Before co-culturing, THP1
127 cells were labelled with a fluorescent tracer dye to distinguish inoculum (MeWo) and
128 target (THP1) cells during flow cytometry analysis (Figure S3A,B). For all experiments,
129 uninfected MeWo cells were additionally used as target cells. MeWo cells do not
130 induce type I IFNs in response to VZV (Figure 1). Infected cells within the target cell
131 population were identified by cell-surface staining for the VZV glycoprotein E
132 (gE)/glycoprotein I (gI) complex (Figure S3B) (Mo et al., 2003).
133 Due to the nature of the co-culture, cells harvested for RT-qPCR and immunoblotting
134 contained both target and inoculum cells. Flow cytometry analysis revealed that across
135 genotypes, target cells constituted between 50% and 85% of all cells in uninfected
136 samples and between 70% and 95% in infected samples (Figure S3C). Amongst target
137 cells, the infected cell population constituted between 10% and 30% of cells (Figure
138 S3D). This showed that all THP1 KO cell lines tested here were permissive for VZV
139 infection.
140
141 ## The Type I IFN Response to VZV Requires the DNA Sensor cGAS
142 To investigate whether THP1 cells induce type I IFNs in response to VZV we analysed
143 mRNA expression levels of *IFNB1* (encodes IFNβ) and *IFI44*, an ISG. In WT THP1
144 cells, both transcripts were robustly induced after VZV infection (Figure 1A). Similar
145 results were obtained using MyD88 KO and MAVS KO cells. In contrast, no

146 transcriptional upregulation of *IFNB1* or *IFI44* was observed in THP1 cells lacking
147 cGAS, STING, TBK1, IRF3, or IFNAR2.
148 Immunoblot analysis showed that the transcription factors STAT1 and STAT2 were
149 only phosphorylated in WT, MyD88 KO, and MAVS KO cells (Figure 1B). In contrast,
150 no p-STAT1 and p-STAT2 signals were observed in cells lacking cGAS, STING, TBK1,
151 IRF3, or IFNAR2. This indicated that only WT, MyD88 KO and MAVS KO cells secreted
152 type I IFNs in response to VZV infection. Consistently, STAT1 and RIG-I, which are
153 both encoded by ISGs, were upregulated at protein level only in the cells showing
154 STAT1/2 activation (Figure 1B). Importantly, we could not observe phosphorylation of
155 STAT1/2 or increased abundance of STAT1 and RIG-I in infected MeWo cells.
156 Western blotting with antibodies against VZV-gE/gI and VZV ORF62 confirmed that all
157 cell lines became infected.
158 Determination of CXCL10 (IP-10) levels in co-culture supernatants confirmed the
159 findings of our RT-qPCR and immunoblot analyses. WT, MyD88 KO, and MAVS KO
160 THP1 cells produced low levels of CXCL10 at baseline and these were increased after
161 infection with VZV (Figure 1C). No CXCL10 was detected in supernatants from
162 uninfected and infected cGAS KO, STING KO, TBK1 KO, and IFNAR2 KO THP1 cells;
163 similarly, MeWo cells did not secrete CXCL10. We could detect low levels of CXCL10
164 in supernatants from IRF3 KO cells but there was no increase above baseline after
165 infection. Collectively these results demonstrate that in THP1 cells the type I IFN
166 response to VZV infection required the DNA sensor cGAS and the STING – TBK1 –
167 IRF3 signalling axis. It is therefore likely that dsDNA is the PAMP recognised in VZV-
168 infected cells.
169
170 **A VZV ORF Expression Library**
171 Type I IFNs inhibit VZV infection (Kim et al., 2017; Ku et al., 2016). VZV, like many other
172 viruses, employs immune evasion strategies that target the type I IFN system. For
173 example, both ORF61 and ORF62 prevent IRF3 activation through distinct
174 mechanisms (Sen et al., 2010; Zhu et al., 2011). In light of our finding that cGAS was
175 crucial for type I IFN induction in response to VZV, we hypothesised that the virus
176 expresses a direct antagonist of cGAS and/or STING. Indeed, other large DNA viruses
177 often encode multiple antagonists of the same innate immune pathway (Smith et al.,
178 2018; Stempel et al., 2019). In order to test the role of individual viral gene products in
179 immune evasion we generated an expression library for all canonical VZV ORFs. All
180 coding sequences were PCR-amplified and cloned into a gateway entry vector. Using
181 recombination, these sequences were then shuttled into a lentiviral vector
182 (pLenti6.3/TO/V5). This vector allows expression with a C-terminal V5 epitope tag
183 either after transient transfection or *via* lentiviral transduction. To validate these
184 constructs, we transiently transfected HEK293T cells and analysed expression of VZV
185 proteins by immunoblot using an antibody against the V5-tag (Figure S4). 59 of 72
186 constructs (82%) were expressed and bands at the expected molecular weights were
187 detected. Five constructs were expressed but at the wrong size, and eight were not
188 expressed at all. This VZV ORF library is a resource for the scientific community and
189 is available to all interested scientists.

190
191 **Identification of ORF9 as an Antagonist of DNA sensing**
192 To investigate whether VZV ORFs block cGAS/STING activation, we utilised a
193 luciferase-based screening platform in HEK293T cells. In brief, a plasmid expressing
194 Firefly luciferase under *IFNB1* promotor control and pRL-TK, which constitutively
195 expresses Renilla luciferase, were transiently transfected. HEK293T cells do not
196 express cGAS and STING naturally. We therefore reconstituted human cGAS and
197 human STING by transient transfection, which results in activation of the *IFNB1*
198 promotor and firefly luciferase expression. Lastly, individual viral ORFs (or controls)
199 were co-expressed. Firefly luciferase expression was normalised to Renilla luciferase
200 expression, and we calculated for each ORF a luciferase fold change to an empty
201 vector control condition without cGAS and STING expression constructs. The mean
202 and standard deviation of all data points was then used to calculate Z-values, which
203 represent the number of standard deviations an individual data point is diverging from
204 the mean. We used these Z-scores to rank ORFs in their ability to block IFN activation
205 downstream of cGAS/STING (Figure 2A). KSHV ORF52, a previously described
206 cGAS-antagonist (Wu et al., 2015), and the L protein of EMCV, a previously described
207 IRF3-antagonist (Freundt et al., 2018), served as positive controls. As expected, we
208 found these with the lowest ranks (i.e. smallest fold change) in our assay and both
209 potently blocked firefly luciferase induction. In addition, we identified a number of VZV
210 ORFs that showed similar behaviour. The two aforementioned IRF3 antagonists
211 expressed by VZV, ORF61 and ORF62, were among them, which further validated our
212 approach.
213 We performed this screening experiment three times; Figure 2B displays the results as
214 a heatmap. We identified a number of ORFs that reproducibly ranked very low. To
215 identify VZV proteins that specifically block the cGAS and/or STING, and not
216 downstream signalling proteins such as IRF3 that are also activated by other PRRs,
217 we compared selected hits from the primary screen in their ability to block reporter
218 activation by overexpression of cGAS/STING or RIG-I-CARD (data not shown). RIG-I-
219 CARD is a constitutively active variant of RIG-I that activates the *IFNB1* promotor *via*
220 MAVS. A direct cGAS/STING antagonist is therefore unable to block this stimulation.
221 We identified the protein encoded by ORF9 of VZV to selectively block reporter
222 activation by cGAS/STING but not RIG-I-CARD when compared to empty vector
223 (Figure 2C).
224 We then aimed to verify that VZV ORF9 has the ability to antagonise activation of
225 cGAS by dsDNA in an endogenous setting. THP1 monocytes were stably transduced
226 with expression constructs for ORF9-V5 or for GFP-V5 as a negative control (Figure
227 2D). We stimulated cGAS in these cells by transfection of increasing doses of dsDNA
228 and measured expression levels of *IFNB1* mRNA and *IFNL1* mRNA (encoding a type
229 III IFN) by RT-qPCR (Figure 2E). As expected, THP1 cells expressing GFP showed a
230 dose-dependent increase in expression of both transcripts. In contrast, cells
231 expressing ORF9 did not respond to low doses of DNA. At higher doses, their response
232 was attenuated when compared to GFP-expressing cells. Collectively, these data
233 revealed that the VZV ORF9 protein prevented cGAS/STING activation.
234

235 **VZV ORF9 Interacts With cGAS**
236 We hypothesised that VZV ORF9 exerts its antagonistic function by directly interacting
237 with either cGAS or STING. To test this, HEK293T cells were transiently transfected
238 with expression constructs for cGAS-FLAG, STING-HA, and ORF9-V5 and protein
239 interaction was analysed by immunoprecipitation (IP). We used antibodies against the
240 epitope tags and analysed IP fractions by immunoblotting (Figure 3A). All ectopically
241 expressed proteins were precipitated efficiently, and an IgG isotype control antibody
242 did not precipitate any of the proteins tested. Interestingly, ORF9 was detected in the
243 bound fraction after cGAS IP. The reverse IP confirmed this result: we found cGAS in
244 the ORF9 IP. In contrast, ORF9 did not interact with STING in this assay (Figure 3A).
245 To verify that this interaction occurred with endogenous cGAS, we used THP1 cells
246 stably transduced to express FLAG-ORF9, which was precipitated from cell lysates
247 with α-FLAG antibody. Indeed, endogenous cGAS was present in the IP fraction; IP of
248 FLAG-GFP served as a negative control (Figure 3B).
249 Next, we asked whether ORF9 expressed from its endogenous promotor during viral
250 infection had the ability to interact with cGAS. We used a recombinant VZV that
251 expressed C-terminally V5-tagged ORF9 from its endogenous genomic locus. We
252 infected THP1 cells and HaCaT cells (a keratinocyte cell line that expresses cGAS)
253 with WT VZV or $VZV^{ORF9\text{-}V5}$ and performed α-V5 IP (Figure 3C). In both THP1 and
254 HaCaT cells infected with $VZV^{ORF9\text{-}V5}$, endogenous cGAS co-precipitated with ORF9.
255 These data showed that endogenous ORF9 protein expressed by the virus in infected
256 cells interacted with cGAS.
257 To investigate whether the two proteins interact in living cells, we overexpressed
258 tagged ORF9 and cGAS in HEK293T cells and performed immunofluorescence
259 analysis (Figure 3D). Expression of ORF9 alone resulted in cytoplasmic staining.
260 Similarly, cGAS was detected in the cytoplasm. We further observed cGAS foci co-
261 localising with extranuclear DNA. Extranuclear DNA foci, sometimes in the form of
262 micronuclei, can be observed in some cancer cells and have been shown to bind cGAS
263 (Harding et al., 2017; Hu et al., 2019; Mackenzie et al., 2017). Interestingly, when ORF9
264 and cGAS were expressed together, both proteins co-localised in DAPI-positive,
265 extranuclear regions. This indicated that ORF9 interacted with cGAS in cells and
266 localised together with cGAS in DNA-positive areas.
267 In order to biochemically characterise the interaction between ORF9 and cGAS in more
268 detail, we performed experiments in a cell-free system. We expressed cGAS, cGAS-
269 HA, FLAG-ORF9, and FLAG-GFP in *E. coli* and performed single-step purification
270 (Figure S5). First, we tested whether ORF9 and cGAS interacted directly using the far
271 western protocol (Figure 3E). FLAG-ORF9 or FLAG-GFP protein were separated on a
272 denaturing SDS-PAGE gel and transferred to a membrane. The proteins on the
273 membrane were then re-natured and incubated with recombinant cGAS as a probe.
274 Possible binding of cGAS to proteins on the membrane was then tested using α-cGAS
275 antibody. Indeed, we found that probing for cGAS resulted in a signal at the size of
276 ORF9 (Figure 3F). Importantly, cGAS did not bind to GFP.
277 We then tested interaction of the two recombinant proteins using immunoprecipitation.
278 FLAG-ORF9 or FLAG-GFP were incubated with cGAS-HA in the test tube. The

279 proteins were then precipitated using antibodies against the epitope tags. Immunoblot
280 analysis of the IP fractions showed that cGAS was co-immunoprecipitated with ORF9
281 but not GFP (Figure 3G). The reverse IP of cGAS resulted in binding of both ORF9
282 and GFP; however, the signal was stronger for ORF9. These data established that
283 VZV ORF9 and cGAS interacted without the requirement for another cellular or viral
284 protein.
285 To gain insight into possible structural features of ORF9 we used the PSIPRED 4.0
286 algorithm to predict its secondary structure based on the amino acid sequence (Buchan
287 and Jones, 2019). This analysis predicted a four sheet - helix motif in the N-terminal
288 region and a two helix - sheet - helix motif in the C-terminal region of ORF9 (Figure
289 4A). Using six ORF9 truncation mutants (Figure 4A), we tested whether these putative
290 structural elements were involved in the interaction with cGAS. Firstly, we
291 overexpressed both human cGAS and ORF9 mutants in HEK293T cells. Consistent
292 with our earlier observation, full-length ORF9 co-immunoprecipitated cGAS. The C-
293 terminal half of ORF9 (construct II) behaved the same, while the N-terminal half
294 (construct I) failed to interact with cGAS. ORF9 constructs III, IV, and V also pulled
295 down cGAS. All ORF9 constructs that interacted with cGAS shared amino acids (AA)
296 151 to 240. Interestingly, this region harbours the predicted two helix - sheet - helix
297 motif. However, IP of $ORF9^{151-240}$ (construct VI) did not co-precipitate cGAS (Figure
298 4B). Secondly, we tested whether endogenous cGAS interacted with selected ORF9
299 truncation mutants stably expressed in THP1 cells. Consistent with the data from
300 HEK293T cells, we found that full-length ORF9 and constructs II and V interacted with
301 endogenous cGAS, while constructs I and VI did not (Figure 4C). Taken together,
302 these biochemical and imaging data established that VZV ORF9 and cGAS were
303 interaction partners. Furthermore, our results suggested that the central portion of
304 ORF9 (construct VI, AA 151-240) was required but not sufficient for this interaction.
305 However, it is also possible that $ORF9^{151-240}$ does not fold correctly in isolation.
306
307 **ORF9 binds DNA**
308 We next considered how ORF9 might block DNA sensing by cGAS and hypothesised
309 that ORF9 binds DNA. We incubated biotinylated VACV-70mer dsDNA with
310 recombinant ORF9; recombinant cGAS and GFP served as positive and negative
311 controls, respectively. The VACV-70mer is a well-established immunostimulatory
312 dsDNA that binds cGAS (Almine et al., 2017; Lum et al., 2018; Unterholzner et al., 2010).
313 The DNA was then precipitated using streptavidin beads and the presence of bound
314 proteins was analysed by immunoblotting (Figure 4D). In the absence of DNA, none of
315 the proteins were precipitated. As expected, cGAS bound to DNA. Interestingly, ORF9
316 also was pulled down by DNA, both alone and in the presence of cGAS. GFP did not
317 bind DNA under any conditions. These data show that ORF9 bound DNA, which may
318 be related to its activity as a cGAS antagonist.
319
320 **VZV ORF9 Prevents cGAMP Synthesis**
321 cGAS activation by dsDNA results in the synthesis of cGAMP. Given our findings that
322 ORF9 blocked DNA sensing and interacted with cGAS and DNA, we next tested

323 whether ORF9 prevents cGAMP production. Transfection of HEK293T cells with
324 plasmids encoding GFP-tagged HIV-1 gag and VSV-G results in the production of
325 VSV-G pseudotyped, HIV-1 GFP-capsid containing virus-like particles (VLPs). Co-
326 expression of cGAS during VLP production leads to the presence of cGAMP within the
327 particles (Bridgeman et al., 2015; Chauveau et al., 2020). We hypothesised that the
328 presence of ORF9 during VLP production blocks cGAS activation and thus prevents
329 the presence of cGAMP in VLPs. We produced VLPs in the presence or absence of
330 cGAS with additional co-transfection of ORF9, or GFP as a negative control (Figure
331 5A). VLP producer cells were analysed by immunoblotting (Figure 5B). Infection of
332 HEK293 cells and quantification of GFP-positive cells by flow cytometry confirmed
333 equivalent infectivity of the different VLP preparations (Figure 5C, S6). The HEK293
334 cells used in this assay endogenously express STING. In response to cGAMP present
335 in VLPs, these cells produce type I IFN, which we measured using a bioassay
336 (Bridgeman et al., 2015; Chauveau et al., 2020). As expected, no type I IFN could be
337 detected in response to infection with VLPs produced in the absence of cGAS (Figure
338 5D). In contrast, particles produced in the presence of cGAS and GFP potently
339 stimulated type I IFN production. The presence of ORF9 during particle production with
340 cGAS completely abrogated type I IFN stimulatory activity. This observation indicates
341 that ORF9 prevented cGAMP production by cGAS.
342

343 **DISCUSSION**

344

345 VZV is a highly prevalent human pathogen, yet little is known for this virus about host-
346 pathogen interactions and innate immunity. Here we report that cGAS and its
347 downstream signalling pathway consisting of STING, TBK1 and IRF3 were required
348 for type I IFN induction after VZV infection. An earlier study using RNA interference
349 had implicated STING in innate recognition of VZV (Kim et al., 2017). Our results confirm
350 this observation by complete genetic ablation, and – importantly – identify cGAS as the
351 DNA sensor for VZV. It is possible that innate sensing pathways that detect VZV differ
352 between cell types. Indeed, a study using inhibitory oligonucleotides found that
353 plasmacytoid DCs produce type I IFN in a partially TLR9-dependent manner (Yu et al.,
354 2011). In contrast, we found that the essential TLR9 adaptor protein MyD88 was
355 dispensable for type I IFN induction in VZV infected THP1 cells. It will be interesting to
356 characterise innate sensing pathways in different cell types relevant to *in vivo* infection,
357 including neuronal cells, T cells and skin cells. This is important because the viral life
358 cycle and effects of viral replication on host cells can differ between cell types (Zerboni
359 et al., 2014). For example, VZV shows cytopathic effects in fibroblast and some immune
360 cells but does not induce cell death in neurons (Gerada et al., 2020). Future investigation
361 should therefore not only address the role of PRRs in induction of cytokines such as
362 type I IFNs but also of cell death.
363 Our identification of cGAS as a sensor of VZV infection implicates recognition of an
364 immunostimulatory DNA in infected cells. Studies of herpesvirus entry suggest that the
365 viral DNA remains within the viral capsid during nuclear targeting and may therefore
366 be unavailable for binding to cGAS (Radtke et al., 2006). Recently, single-cell analysis
367 of HSV-1 infection showed that only cells undergoing abortive infection respond by
368 production of type I IFNs (Drayman et al., 2019). It is therefore possible that viral particles
369 with defective capsids are responsible for the type I IFN response observed in bulk
370 populations of cells. Furthermore, cellular restriction mechanisms may make viral DNA
371 from capsids accessible for cGAS binding. Indeed, degradation of herpesviral capsids
372 *via* the ubiquitin – proteasome system has been suggested to release viral DNA for
373 recognition (Horan et al., 2013). Alternatively, cellular DNA may induce type I IFN.
374 Indeed, infections with multiple different viruses result in the accumulation of
375 extranuclear DNA and in mitochondrial damage (Ablasser and Chen, 2019). Host DNA
376 has been shown to stimulate cGAS in the context of HSV-1 infection (West et al., 2015).
377 Whether viral and/or cellular DNA species activate cGAS in VZV-infected cells should
378 be tested in the future by deep sequencing of cGAS-bound DNA. However, this
379 approach has thus far been hampered by the lack of suitable antibodies for specific
380 cGAS IP.
381 We further describe the identification of ORF9 as a cGAS antagonist. ORF9 interacted
382 with cGAS in a variety of assays, and blocked cGAMP production and DNA-triggered
383 type I IFN induction. ORF9 is a tegument protein, making it an attractive candidate for
384 antagonising innate immunity. Tegument proteins are contained within viral particles
385 and are delivered into cells at the same time as viral DNA. ORF9 may therefore prevent
386 DNA sensing during early infection before viral gene expression. We speculate that

387 ORF9 exerts its function by disrupting cGAS-DNA interactions. Formation of multimeric
388 complexes and higher order structures of cGAS and DNA facilitate cGAS activation
389 (Andreeva et al., 2017; Du and Chen, 2018; Li et al., 2013; Zhang et al., 2014; Zhou et al.,
390 2018). We show that ORF9 binds DNA, which may prevent formation of cGAS
391 multimers (Andreeva et al., 2017). It is possible that ORF9 simply outcompetes cGAS by
392 binding to DNA. However, we favour a model in which direct protein-protein
393 interactions between the ORF9 and cGAS, as well as ORF9 – DNA interactions may
394 prevent cGAS from forming higher order complexes. Future experiments will be
395 required to decipher in detail the relationships between ORF9, cGAS, DNA, and
396 cGAMP production. This should include testing the DNA length required for this given
397 that cGAS oligomer formation is critically dependent on DNA length (Andreeva et al.,
398 2017; Li et al., 2013; Luecke et al., 2017; Zhou et al., 2018).
399 ORF9 is essential for viral replication and is a member of the $\alpha$-herpesvirus UL49 gene
400 family (Che et al., 2008; Tischer et al., 2007). With its closest relative, HSV-1 VP22, it
401 shares 36% AA sequence similarity (Hew et al., 2015). ORF9 has well-established roles
402 in VZV nuclear egress and secondary envelopment (Che et al., 2013; Lebrun et al., 2018;
403 Riva et al., 2013; Riva et al., 2015). Mutational analyses have attributed these functions
404 to amino acids or regions either in the N-terminal half or the extreme C-terminus of the
405 protein, whilst we describe a central region (AA151-240) to be required for the
406 interaction of ORF9 with cGAS. A crystal structure is available for the core domain of
407 HSV-1 VP22 that is homologous to this region of ORF9 (Hew et al., 2015). The HSV-1
408 VP22 core folds into a two helix - sheet - helix confirmation. Hew et al. further describe
409 structural similarity between HSV1 VP22 and the unrelated MHV68 ORF52 (Hew et al.,
410 2015). MHV68 ORF52 is the homologue of KSHV ORF52. Secondary structure
411 prediction and examination of the published crystal structures revealed that VZV
412 ORF9, HSV1 VP22, KSHV ORF52, and MHV68 ORF52 all potentially share a two helix
413 – sheet structural feature (Figure S7). Interestingly, both HSV-1 VP22 and KSHV
414 ORF52 have been described previously to inhibit cGAS activation (Huang et al., 2018;
415 Wu et al., 2015). Antagonism of cGAS by KSHV ORF52 required its DNA binding
416 properties. Collectively, these observations lead us to put forward a model in which
417 distantly related herpesviruses have retained within unrelated proteins a structural
418 feature that confers cGAS antagonist properties. Alpha, beta, and gamma-
419 herpesviruses have been estimated to have evolutionarily diverged hundreds of
420 millions of years ago (Brito and Pinney, 2018; Davison, 2002; McGeoch et al., 1995).
421 Anemone species that have diverged from humans more than 500 million years ago
422 harbour cGAS-like enzymes (Kranzusch et al., 2015). This indicates that a common
423 ancestral organism expressed such proteins. It further opens up the possibility that
424 ancient herpes viruses evolved the relevant evasion strategies. We hypothesise that
425 antagonism of cGAS by herpesviruses constitutes an ancient molecular mechanism
426 that evolved long before the advent of antiviral cytokines and IRF3 during evolution.
427

## AUTHOR CONTRIBUTIONS

JH, RER and JR conceived the study, designed experiments and analysed data. JH, SR, CC, LC and TD performed experiments. JH and RER developed methodology. JH and JR wrote the manuscript. All authors read and approved the final manuscript.

## ACKNOWLEDGMENTS

The authors thank J Cohen, C Sadzot and S Paludan for VZV stocks, antibodies and cell lines, and P Hublitz and Z Holloway (MRC WIMM Genome Engineering Facility) for their help with CRISPR plasmid generation. The authors further thank C Reis e Sousa, F Zhu, G Ogg, L Unterholzner, A Pichlmair, G Towers, T Fujita, J Haas, and M Reijns for reagents and advice. The authors thank M Brinkmann, J McKeating, and members of the Rehwinkel lab for critical discussion.

## FUNDING

This work was funded by the UK Medical Research Council [MRC core funding of the MRC Human Immunology Unit] and by the Wellcome Trust [grant number 100954]. JH was supported by the European Commission under the Horizon2020 program H2020 MSCA-ITN GA 675278 EDGE. The MRC WIMM Genome Engineering Facility is supported by grants from the MRC/MHU (MC_UU_12009), the John Fell Fund (123/737) and by MRC WIMM Strategic Alliance awards G0902418 and MC_UU_12025. The funders had no role in study design, data collection and analysis, decision to publish, or preparation of the manuscript.

## CONFLICT OF INTEREST

The authors declare no conflict of interest.

# FIGURES

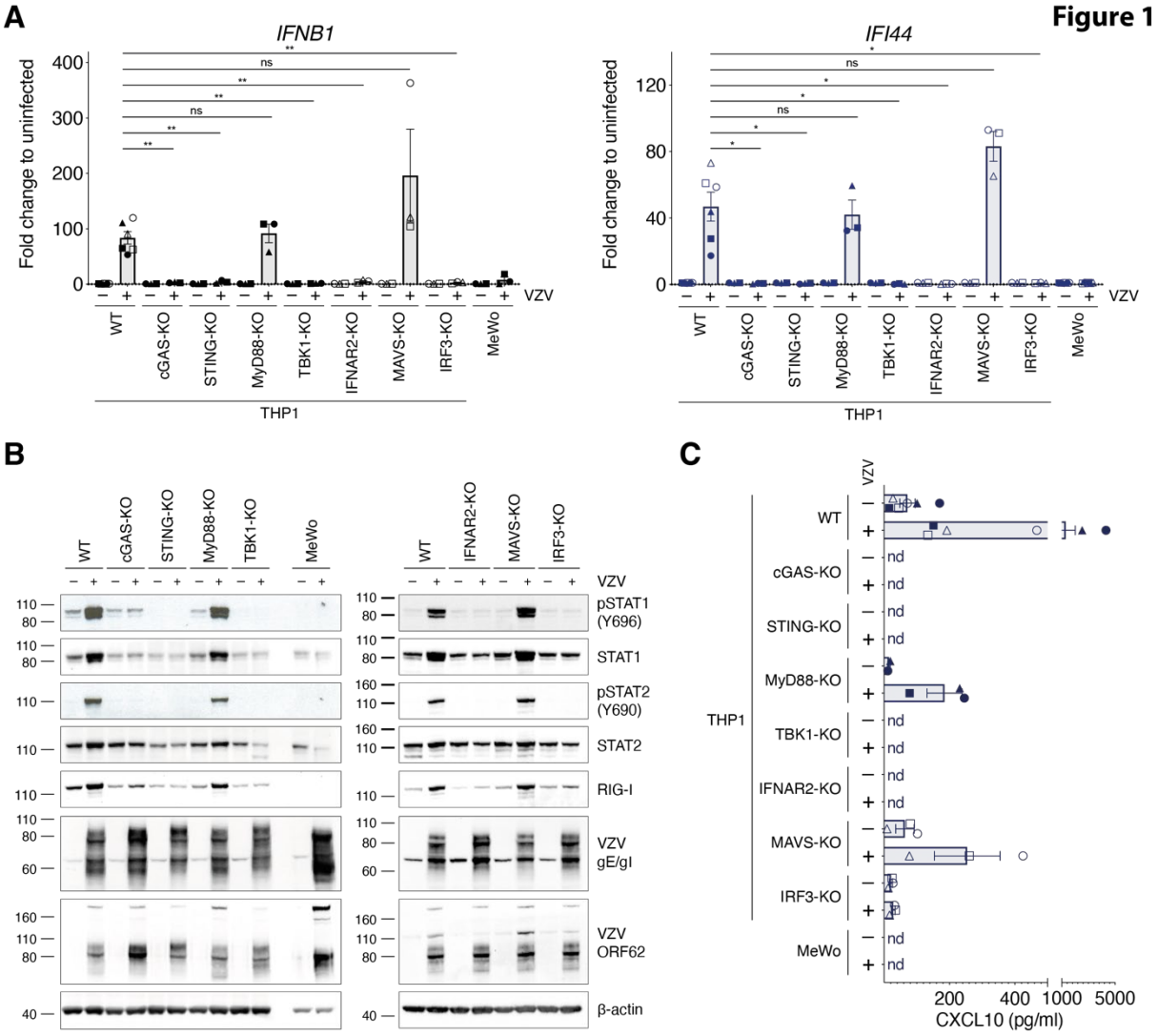


**Figure 1. The cGAS/STING DNA sensing pathway induces type I IFNs in response to VZV infection.**
**(A)** THP1 cells of the indicated genotypes were mock infected or infected with VZV by co-culture as described in Figure S3. The mRNA expression levels of *IFNB1* (encoding IFNβ) and *IFI44* were analysed by RT-qPCR. Expression levels were normalised to *GAPDH* and are shown as fold changes relative to levels in uninfected cells. **(B)** Cells were infected as in (A) and were analysed by western blot using the indicated antibodies. **(C)** Levels of CXCL10 (IP-10) in co-culture supernatants were quantified by ELISA.
Panels (A) and (C) show pooled data from six (THP1 WT, MeWo) or three (THP1 KOs) independent biological repeats (n=3/6 ± SEM). The different shapes of data points correspond to independent biological repeat experiments. Panel (B) shows a representative result of three independent repeats. Statistical analysis in panel (A) was one-way ANOVA with Dunnett's multiple comparisons test. **=p<0.01, *=p<0.05, ns=not significant.

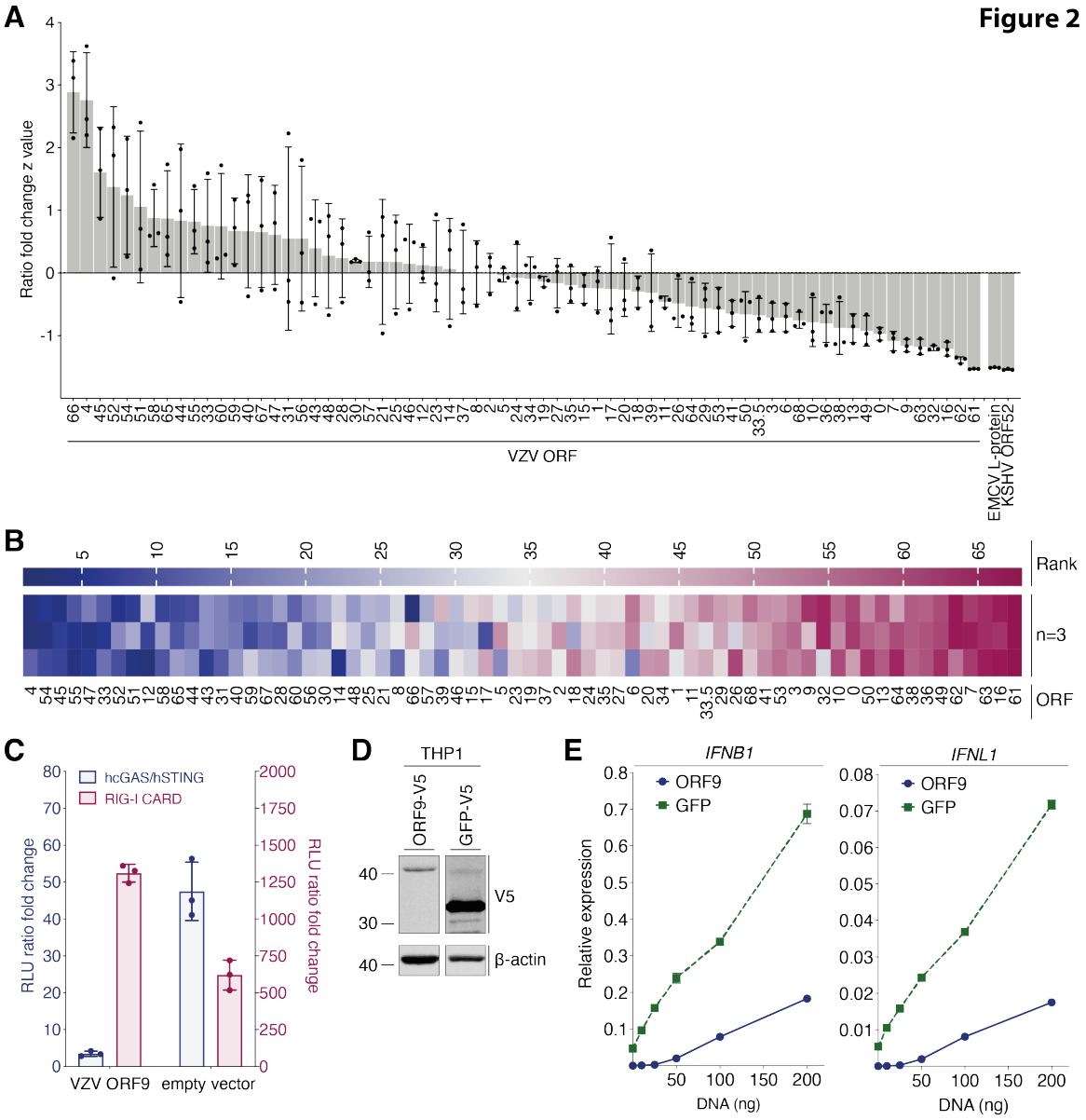


**Figure 2. Screening of all VZV ORFs identifies ORF9 as an antagonist of cGAS-mediated DNA sensing.** **(A)** HEK293T cells were transfected with p125-F-Luc, pRL-TK, expression plasmids for human cGAS and human STING, as well as expression plasmids for individual VZV ORFs. The next day luciferase activity was determined. For each ORF a Z-value was calculated and ORFs were sorted in descending order. **(B)** The experiment shown in (A) was repeated three times and for each ORF in each experiment a rank was determined (highest Z-value = rank 1). Ranks are displayed as a heatmap. The order of the ORFs in the heatmap was determined by their average rank. **(C)** HEK293T cells were transfected as in (A) with expression constructs for VZV ORF9 or empty vector. In parallel, reporter expression was stimulated by co-transfection of the RIG-I-CARD plasmid instead of hcGAS and hSTING. A luciferase fold change was calculated to unstimulated cells. **(D)** Immunoblot analysis of THP1 cells stably transduced with either VZV ORF9-V5 or GFP-V5. **(E)** The same cells as in (D) were PMA-differentiated and transfected with the indicated doses of dsDNA. Expression of *IFNB1* and *IFNL1* mRNAs was assessed by RT-qPCR. Graphs show expression relative to *GAPDH*.

Panel (A) is representative of three independent experiments, which are summarised in panel (B). Panels (C) and (D) are representative of two independent experiments. Data points are technical triplicates with mean and standard deviation (A, C) or the average of technical duplicates with range (D).

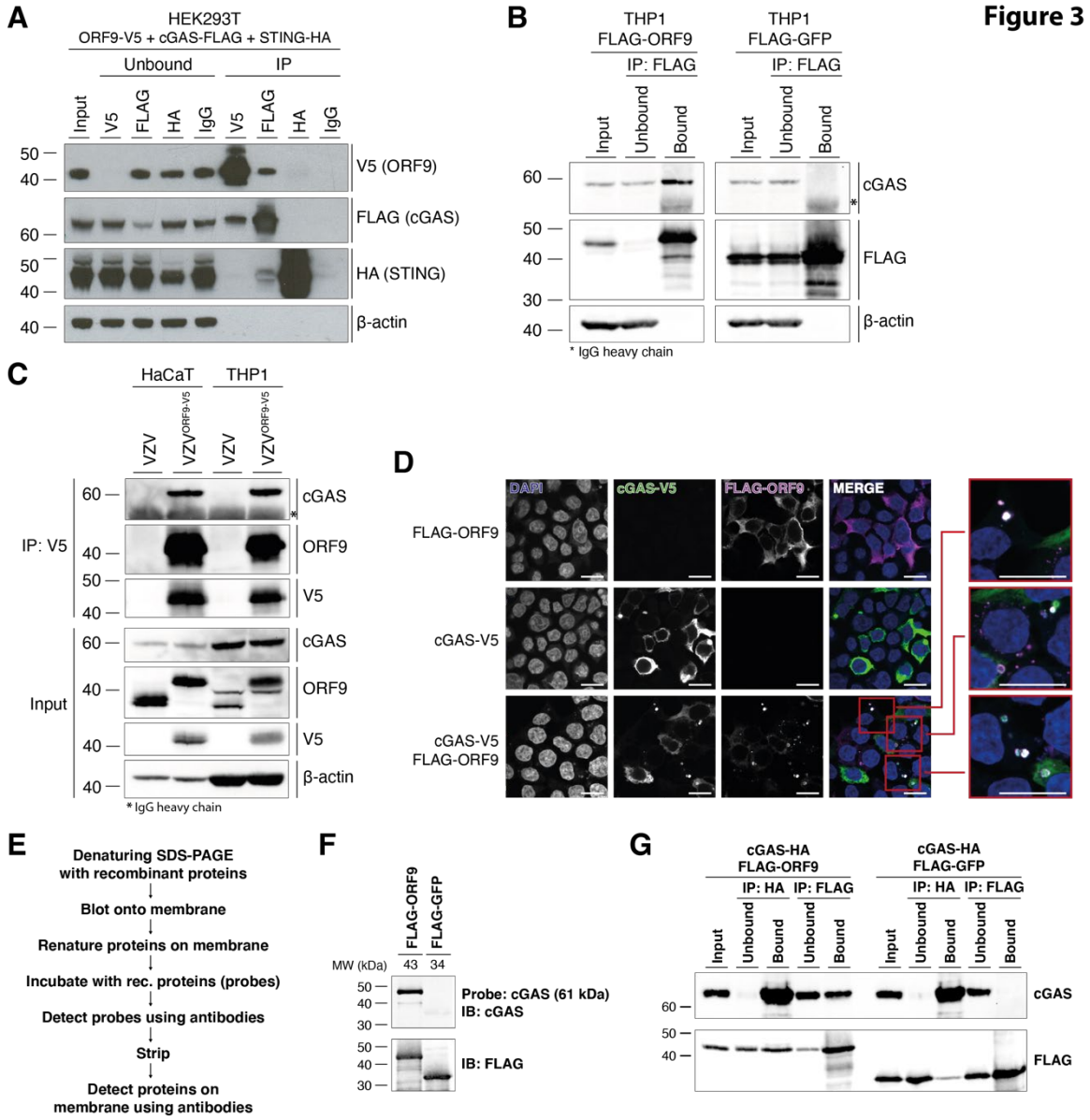


**Figure 3. ORF9 interacts with cGAS.**

**(A)** HEK293T cells were transfected with expression plasmids for ORF9-V5, human cGAS-FLAG, and human STING-HA. The next day, cells were lysed and overexpressed proteins were immunoprecipitated with α-V5, α-FLAG, α-HA, or IgG isotype control antibody. Input, unbound and IP fractions were subjected to immunoblotting using the indicated antibodies. **(B)** THP1 monocytes stably transduced with either VZV FLAG-ORF9 or FLAG-GFP were PMA-differentiated overnight. The next day, cells were lysed and ectopically expressed proteins were immunoprecipitated using α-FLAG antibody. Input, unbound and IP fractions were subjected to immunoblotting using the indicated antibodies. **(C)** HaCaT cells and PMA-differentiated THP1 cells were infected with WT VZV or VZV$^{ORF9\text{-}V5}$ through co-culture with infected MeWo cells for 48 hours. Cells were lysed and ORF9 was immunoprecipitated using α-V5 antibody. Input and IP fractions were subjected to immunoblotting using the indicated antibodies. **(D)** HEK293T cells were seeded onto glass coverslips and were transfected with human cGAS-V5, FLAG-ORF9, or both together. The next day, cells were fixed, permeabilised and stained using α-V5-FITC, rabbit-α-FLAG, and goat-α-rabbit-AF647 antibodies, and DAPI. Mounted coverslips were imaged using confocal microscopy. Scale bars: 15μm. **(E)** Outline of the far western protocol. **(F)** Far western analysis of cGAS-ORF9 interaction. Recombinant FLAG-ORF9 and FLAG-GFP protein were run on an SDS-PAGE gel and transferred to a membrane. After renaturation of proteins, the membrane was incubated with recombinant human cGAS as a probe, which was detected using α-cGAS antibody. After stripping, the proteins on the membrane were detected using α-FLAG antibody. **(G)** Recombinant human cGAS-HA was mixed with recombinant FLAG-ORF9 or FLAG-GFP. Proteins were immunoprecipitated using α-HA and α-FLAG antibodies. Input, unbound and IP fractions were analysed by immunoblotting.

Panels (A) and (G) are representative of two independent experiments. Panels (B), (D), and (F) are representative of three independent experiments. Panel (C) is representative of two (HaCaT) and three (THP1) independent experiments.

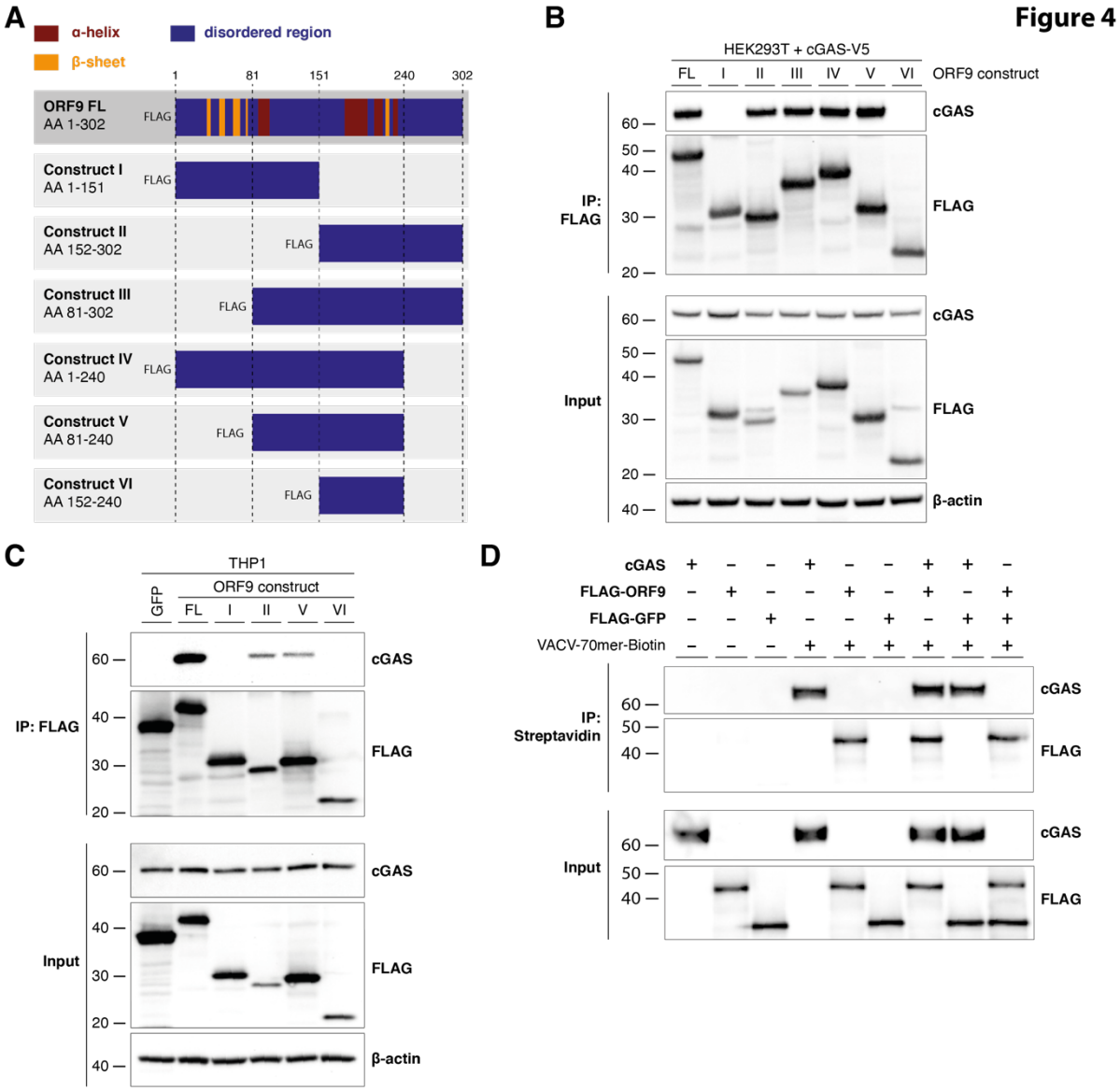


**Figure 4. ORF9 binds DNA and interacts with cGAS *via* its central region.**
**(A)** Schematic showing the ORF9 truncation mutants used in (B) and (C). Secondary structure features are based on predictions made using predictprotein.org (see methods). **(B)** HEK293T cells were transfected with human cGAS-V5 and full-length FLAG-ORF9, or different FLAG-tagged ORF9 truncation mutants. ORF9 constructs were immunoprecipitated using α-FLAG antibody. Input and IP fractions were subjected to immunoblotting using the indicated antibodies. **(C)** THP1 cells were stably transduced with FLAG-GFP, full-length FLAG-ORF9, or different FLAG-tagged ORF9 truncation mutants. ORF9 constructs were immunoprecipitated using α-FLAG antibody. Input and IP fractions were subjected to immunoblotting using the indicated antibodies. **(D)** Recombinant cGAS, FLAG-ORF9, FLAG-GFP, and biotinylated VACV-70mer dsDNA were incubated in the indicated combinations. Lysates were precipitated using streptavidin beads. Fractions were analysed by immunoblotting using the indicated antibodies.
Panel (B) is representative of two independent experiments. Panels (C) and (D) are from one experiment.

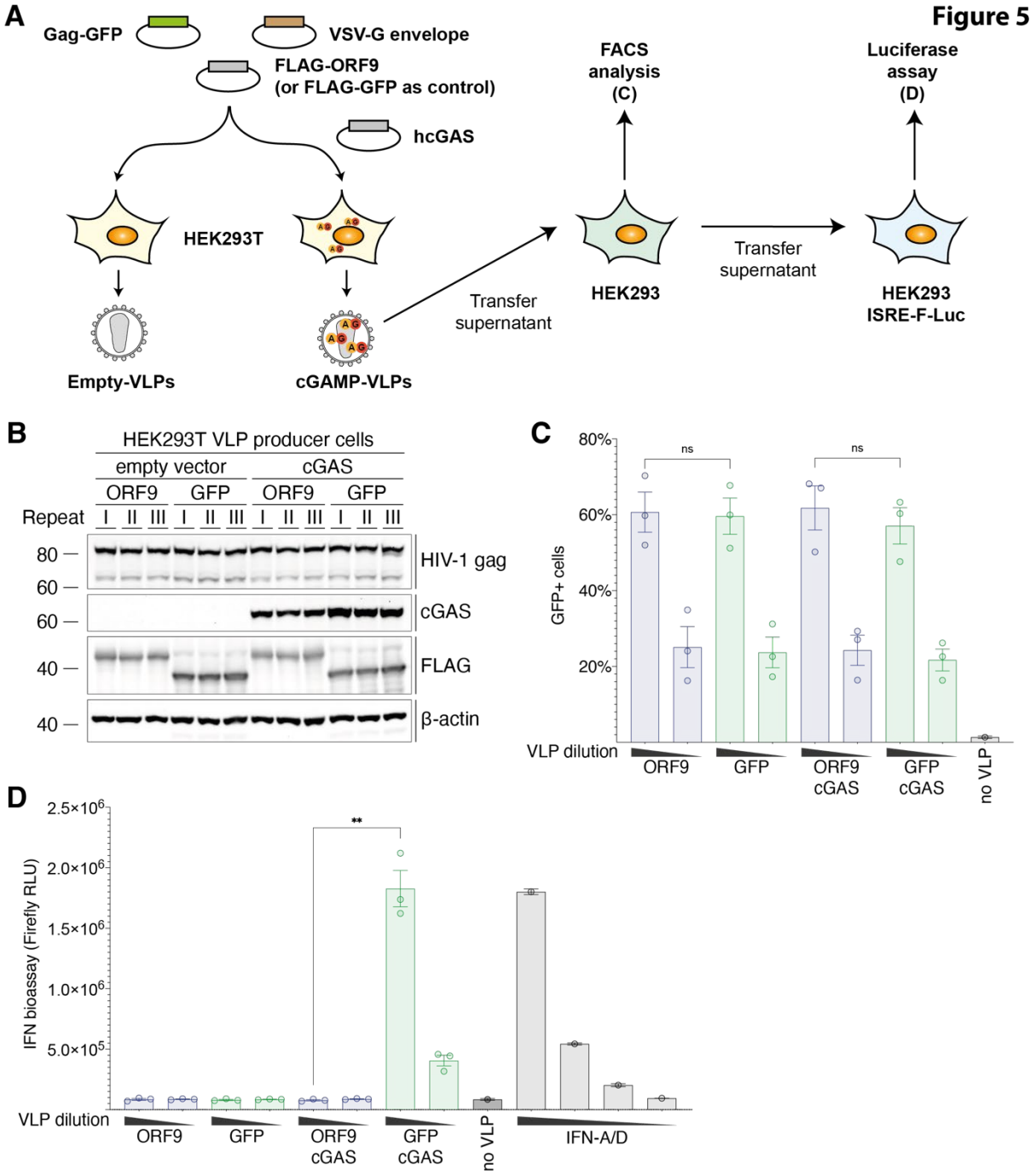


**Figure 5. VZV ORF9 prevents cGAMP-loading of VLPs.**
**(A)** Schematic of the experimental procedure. **(B)** HEK293T cells were transfected with plasmids encoding HIV-1 gag-GFP, VSV-G, FLAG-ORF9 or FLAG-GFP, and human cGAS or empty vector. Supernatants containing VLPs were harvested, and cells were lysed for immunoblotting using the indicated antibodies. **(C)** HEK293 cells were incubated with VLP containing supernatants (neat or diluted 1:2). The next day, cells were harvested and analysed by flow cytometry. The percentage of $GFP^+$ cells is shown. **(D)** HEK293 cell supernatants from (C) were added onto HEK293-ISRE-F-Luc cells. Recombinant IFN-A/D was used as a control (12.5, 6.25, 3.125, and 0 U/ml). After overnight incubation, firefly luciferase activity was determined.
The experiment was repeated three times. In panel (B), lysates from all three repeats were analysed. Panels (C) and (D) show pooled data (mean ± SEM). Statistical analysis: paired, two-tailed t-test, **=p<0.01, ns=not significant.

547 # MATERIALS AND METHODS
548
549 *Cells*
550
551 All cells were cultured at 37°C and 5% $CO_2$ and checked regularly for mycoplasma
552 contamination. Adherent cells were passaged using Trypsin-EDTA (0.25%)
553 dissociation reagent (Gibco) at appropriate confluence. FCS was obtained from Sigma-
554 Aldrich. HEK293 and HEK293T cells (gifts from Caetano Reis e Sousa, The Francis
555 Crick Institute, UK) were maintained in DMEM (Sigma-Aldrich) containing 4.5 g/L
556 glucose, supplemented with 10% (v/v) FCS and 2mM L-glutamine (Gibco) (DMEM
557 complete). HEK293-ISRE-Firefly luciferase reporter cells (clone 3C11) were described
558 previously (Bridgeman et al., 2015). HaCaT cells were a gift from Leonie Unterholzner
559 (Lancaster University, UK) and were maintained in DMEM complete medium. MeWo
560 cells were a gift from Graham Ogg (University of Oxford, UK) and were maintained in
561 MEM supplemented with 10% (v/v) FCS, 2mM L-glutamine (Gibco), 1x Non-essential
562 amino acids (Gibco), and 1mM sodium pyruvate (Gibco). THP1 Dual cells (WT,
563 MyD88-KO, and IFNAR2-KO) were from Invivogen. cGAS-KO, STING-KO, and TBK1-
564 KO THP1 cells were a gift from Soren Paludan (Aarhus University, Denmark) (Holm et
565 al., 2016). MAVS-KO and IRF3-KO cells were generated on the THP1 Dual background
566 as described below. All THP1 cell lines were maintained in RPMI (Sigma Aldrich)
567 supplemented with 10% (v/v) FCS and 2mM L-glutamine (Gibco).
568
569 *Viruses*
570
571 VZV rOka (cosmid-derived recombinant pOka) was a gift from Jeffrey Cohen (NIH,
572 Bethesda, USA) (Cohen and Seidel, 1993). The virus was maintained in monolayers of
573 MeWo cells. In brief, monolayers of infected cells were monitored microscopically for
574 cytopathic effect. Cells that showed high level of infection were detached and infected
575 cells were mixed at appropriate ratios (1:2-1:4) with uninfected cells and re-plated.
576 Aliquots of infected cells were cryopreserved in freezing medium (90% FCS, 10%
577 DMSO), stored in liquid nitrogen, and thawed for experiments. $VZV^{ORF9\text{-}V5}$ is a
578 recombinant virus, in which a C-terminal V5 tag was added to the coding sequence of
579 ORF9. The virus was a kind gift from Catherine Sadzot (University of Liege, Belgium)
580 (Riva et al., 2013).
581
582 *Plasmids*
583
584 The p125-Luc plasmid (*hIFNB1* promotor firefly luciferase) was a gift from T. Fujita
585 (Kyoto University, Japan) (Yoneyama et al., 2004). pRL-TK was from Promega. RIG-I-
586 CARD was a gift from Andreas Pichlmair (Technical University Munich, Germany).
587 pCMV-VSV-G was a gift from Bob Weinberg (Addgene number 8454). The lentiviral
588 packaging plasmid p8.91 was a gift from Greg Towers (University College London).
589 pGag-eGFP was from the NIH AIDS reagent programme (number 11468).
590 pX458/Ruby/MAVS was described previously (Hertzog et al., 2018). pCMV-3tag-KSHV-

591 ORF52 was a kind gift from Fanxiu Zhu (Florida State University, USA).
592 pX458/Ruby/IRF3 was created as described for the MAVS-targeting plasmid. A sgRNA
593 targeting exon 3 of the IRF3 locus was designed using the MIT algorithm
594 (crispr.mit.edu) and cloned into the px458 vector. The pLenti6.3/EMCV-L-V5 plasmid
595 was described previously (Hertzog et al., 2018).
596
597 *Cloning*
598
599 Mammalian expression plasmids for hcGAS and hSTING were created by PCR-
600 amplification using THP1 cDNA and ligation into the gateway entry vector pCR8.
601 Coding sequences were shuttled into expression vectors (pLenti6.3/C-V5,
602 pcDNA3.2/C-FLAG, pcDNA3.2/C-HA) *via* Gateway recombination. Mammalian
603 expression plasmids for eGFP (pLenti6.3/puro/N-FLAG, pDEST31/N-FLAG) were
604 created in a similar way by PCR amplification from pGag-eGFP introducing a stop
605 codon. VZV ORF9 expression plasmids (pLenti6.3/puro/N-FLAG, pDEST31/N-FLAG)
606 were created by amplification of ORF9 with a stop codon and gateway recombination.
607 Expression plasmids for ORF9 truncation mutants (pLenti6.3/puro/N-FLAG) were
608 created by PCR amplification of the respective coding sequence with a start and stop
609 codon. Bacterial expression vectors for FLAG-ORF9, FLAG-GFP, and hcGAS-HA
610 were created by PCR-amplification of the coding sequences from existing plasmids
611 and restriction enzyme cloning into pGEX6P1. pGEX6P1 and pGEX6P1-hcGAS were
612 a kind gift from Martin Reijns (University of Edinburgh, UK). All primer sequences are
613 listed in Table S1.
614
615 *VACV 70mer-Biotin dsDNA*
616
617 A 70bp immunostimulatory dsDNA fragment from VACV was described previously
618 (Unterholzner et al., 2010). Two complementary oligos were synthesised (Sigma Aldrich)
619 and combined at equal molar ratio. The solution was heated to 95°C and allowed to
620 anneal by cooling to RT.
621 Forward sequence:
622 5'-ccatcagaaagaggtttaatatttttgtgagaccatcgaagagagaaagagataaaactttttacgact-3'-
623 TEG-Biotin
624 Reverse sequence:
625 5'- agtcgtaaaaaagttttatctctttctctcttcgatggtctcacaaaaa-tattaaacctctttctgatgg-3'
626
627 *Antibodies*
628
629 For immunoblot: beta-actin-HRP (AC-15, Sigma Aldrich), FLAG-HRP (clone M2,
630 Sigma Aldrich), V5-HRP (R961-25, Invitrogen), RIG-I (Alme1, Calteg Medsystems),
631 VZV gE/GI (MAB8612, GE Healthcare), VZV ORF62 (C05107MA, Meridian Life
632 Science), pSTAT1 (Y701) (58D6, CellSignaling Technology), STAT1 (42H3,
633 CellSignaling Technology), pSTAT2 (D3P2P, CellSignaling Technology), STAT2
634 (D9J7L, CellSignaling Technology), hcGAS (D1D3G, CellSignaling Technology),
635 hSTING (D2P2F, CellSignaling Technology), MyD88 (D80F5, CellSignaling

636 Technology), TBK1 (D1B4, CellSignaling Technology), MAVS (ALX-210-929-C100,
637 ENZO Life Science), IRF3 (D6I4C, CellSignaling Technology), VZV ORF9 (polyclonal
638 rabbit serum, kind gift from Catherine Sadzot (University of Liege, Belgium) (Riva et al.,
639 2013), donkey-anti-mouse-HRP (NA931, GE Healthcare), donkey-anti-rabbit-HRP
640 (NA931, GE Healthcare). For IP: FLAG (clone M2, Sigma Aldrich, V5 (680602,
641 Biolegend), HA (2-2.2.14, Invitrogen). For IF: V5-FITC (R963-25, Invitrogen), FLAG
642 (D6W5B, CellSignaling Technology), goat-anti-rabbit-AF647 (A21246, Invitrogen). For
643 FACS: VZV gE/gI (see above) was conjugated to FITC using FITC Conjugation Kit
644 (Abcam).
645
646 *VZV ORF Library*
647
648 Primers for PCR amplification of individual VZV ORF sequences were designed based
649 on an annotated VZV genome sequence (GenBank accession: AB097933.1). Forward
650 primers included a Kozak sequence (GCCGCC), added before the start codon of an
651 ORF. Reverse primers excluded the Stop codon to allow for addition of a C-terminal
652 tag through the vector (see below). Primer sequences are listed in Table S2. The PCR
653 template was generated by extracting RNA from VZV infected MeWo cells using
654 QIAshredder (Qiagen) and RNeasy Mini Kit (Qiagen). The RNA was reverse
655 transcribed into cDNA using SuperScript II Reverse Transcriptase (Invitrogen). For
656 some ORFs, DNA from infected MeWo cells extracted with DNeasy Blood and Tissue
657 Kit (Qiagen) served as the PCR template. PCR products were generated using
658 Phusion High-Fidelity DNA Polymerase (New England Biolabs) or Herculase II Fusion
659 DNA Polymerase (Agilent Technologies). PCR reactions were analysed by agarose
660 gel electrophoresis and PCR products of the predicted size were extracted from the
661 gel using QIAquick Gel Extraction Kit (Qiagen). Fragments were ligated into the
662 pCR8/TOPO Gateway entry vector (Invitrogen). Plasmid DNA from single clones of
663 transformed *E.coli* (New England Biolabs) was analysed for correct orientation of the
664 insert by Sanger sequencing. Inserts were then shuttled into pLenti6.3/TO/V5-DEST
665 (Invitrogen) using LR Clonase II Enzyme Mix (Invitrogen) for Gateway recombination.
666 All clones with the pLenti6.3/TO/V5 backbone were propagated in recombination-
667 deficient Stbl3 bacteria (Invitrogen).
668 Cloning of the entire coding sequence of ORF22 (8256 bp) was unsuccessful using
669 various amplification and cloning technologies. Therefore, two Gateway entry vectors
670 encoding individual segments within the ORF22 coding sequence (ORF22A: nt 2219-
671 4029, ORF22B: nt 4012-6114, described previously (Uetz et al., 2006)) were used (kind
672 gift from Jurgen Haas, University of Edinburgh, UK). Expression vectors with the
673 pLenti6.3/TO/V5 backbone were generated as described above.
674 To validate expression, HEK293T were seeded at $5x10^5$ cells per well in 12-well plates.
675 The next day, cells were transfected with 600ng VZV ORF or control expression
676 plasmids using 3µl Lipofectamine 3000 (Invitrogen) per well. 24 hours later, cells were
677 lysed in RIPA buffer (10mM TRIS-HCl pH8, 140mM NaCl, 1% Triton-X 100, 0.1% SDS,
678 0.1% sodium deoxycholate, 1mM EDTA, 0.5mM EGTA). Lysates were clarified by
679 centrifugation and 30µg protein was subjected to immunoblotting.

680
681 *IFN Reporter Assay*
682
683 HEK293T cells were seeded at $3.5x10^4$ cells per well in 96-well plates. On the following
684 day, cells were transfected with the following plasmids using Lipofectamine 2000
685 (Invitrogen): 20ng p125-F-Luc, 5ng pRL-TK, 1ng hcGAS, 25ng hSTING, and 50ng of
686 a VZV ORF. Alternatively, cells were transfected with 5ng RIG-I-CARD plasmid instead
687 of cGAS and STING plasmids. The next day, expression of firefly and renilla
688 luciferases was assessed using Dual Luciferase assay system (Promega).
689
690 *Lentivirus Production and Transduction*
691
692 $1.2x10^7$ HEK293T cells were seeded in 15cm cell culture dishes. The next day, cells
693 were transfected with 9µg lentiviral expression plasmids harbouring the gene of
694 interest, 9µg p8.91 plasmid, and 3µg pVSV-G using Lipofectamine 2000. 16 hours
695 later, medium was replaced with fresh growth medium. 24 hours later, lentivirus
696 containing supernatant was harvested, clarified by centrifugation, and stored at 4°C.
697 Cells were overlaid with fresh growth medium. 8 hours later, supernatants were
698 harvested again and pooled with previous supernatants. After 16 hours, lentivirus
699 containing supernatants were harvested for a third time. Pooled supernatants from all
700 three harvests were filtered through a 0.45µm filter, aliquoted into cryovials and stored
701 at -80°C. For transduction of cells, polybrene (Sigma Aldrich) was added to lentiviral
702 supernatants to a final concentration of 8µg/ml. THP1 cells were pelleted and
703 resuspended in lentiviral supernatant containing polybrene. The next day, cells were
704 pelleted and resuspended in fresh growth medium. After overnight incubation, cells
705 were once again pelleted and resuspended in growth medium containing 10µg/ml
706 blasticidin or 1µg/ml puromycin (both Gibco) depending on which vector was used.
707 Surviving cells were used for experiments.
708
709 *cGAMP-loaded VLPs*
710
711 Empty VLPs or VLPs which incorporated cGAMP were generated using a modified
712 procedure based on a previously described method (Bridgeman et al., 2015). $1.4x10^6$
713 HEK293T cells were seeded per well in 6-well plates. The next day, cells were
714 transfected with 2µg of plasmids pDEST31/FLAG-ORF9 or pDEST31/FLAG-GFP, 1µg
715 pGag-eGFP (NIH AIDS reagent program), 500ng pVSV-G, and 1µg of
716 pcDNA3.2/hcGAS or pcDNA3.2/empty-vector. VLPs were harvested as described
717 above. At the end of VLP production, cells were lysed in RIPA buffer and analysed by
718 immunoblotting.
719 $1.75x10^5$ HEK293 cells were seeded per well in 24-well plates. The next day, cells were
720 overlaid with VLP solutions neat or 1:2 diluted in DMEM in the presence of 8µg/ml
721 polybrene (Sigma Aldrich) in duplicate. 16 hours later, supernatants were used for IFN
722 bioassay (see below). The cells were resuspended in PBS and stained with 1µg/ml
723 DAPI (Sigma Aldrich) in PBS for 10min. Cells were washed, fixed with BD CellFix (BD)
724 and analysed immediately on Attune NxT Acoustic Focusing Cytometer (Thermo

725 Fisher). Cells were gated on single, live events. A $GFP^+$ gate was set based on
726 uninfected cells.
727
728 *IFN Bioassay*
729
730 Type I IFN in cell culture supernatants was measured using HEK293-ISRE-Firefly
731 luciferase reporter cells (clone 3C11) as described previously (Bridgeman et al., 2015).
732 $4x10^4$ 3C11 cells were seeded per well into 96-well plates in growth medium. The next
733 day, test supernatants were clarified by centrifugation and overlaid onto 3C11 cells
734 seeded before. A standard consisting of 2-fold dilutions of recombinant IFN-A/D
735 (Sigma-Aldrich) was analysed in parallel. After overnight incubation reporter activation
736 in 3C11 cells was assessed by measuring luciferase activity using ONE-Glo luciferase
737 assay (Promega).
738
739 *THP1 Knockout Cell Generation*
740
741 For generation of knockout cells using CRISPR/Cas9 technology the pX458-mRuby
742 plasmid encoding the Cas9 protein, the sgRNA, and mRuby was used (Hertzog et al.,
743 2018). $1x10^7$ THP1 cells were transiently transfected with 50µg of respective pX458
744 plasmids using Lipofectamine LTX (Invitrogen) and incubated overnight. The next day
745 cells were stained with 10µg/ml DAPI in PBS for 10min. After resuspension of cells in
746 growth medium, live, mRuby-positive cells were FACS-sorted into eppendorf tubes
747 containing growth medium with 20% FCS. The suspension of sorted cells was diluted
748 with special growth medium (50% conditioned THP1 medium, 40% fresh RPMI with
749 10% FCS, 10% additional FCS) to one or three cells per 200µl. 200µl cell suspension
750 were then dispensed into each well of a 96-well plate (one or three cells per well). The
751 cells were incubated for several weeks until clones grew out.
752 The absence of the targeted protein in each clone was assessed by immunoblot
753 analysis. For functional validation, $1.5x10^5$ cells were seeded per well into 96-well
754 plates in growth medium containing 10ng/ml PMA (Sigma-Aldrich). The next day cells
755 were transfected with 5ng IVT-RNA (Rehwinkel et al., 2010) or 15ng *E.coli* DNA
756 (Invivogen) using Lipofectamine 2000 (Invitrogen). 24 hours later, IFN in supernatants
757 was measured using the type I IFN bioassay. Knockout clones were further analysed
758 for insertions and deletions in their genomic loci. *MAVS* and *IRF3* target regions were
759 PCR-amplified using Herculase II Fusion DNA Polymerase. PCR amplicons were gel
760 extracted (QIAquick Gel Extraction Kit) and sequenced by Sanger sequencing.
761 Sequencing traces were analysed using the TIDE software (https://tide.nki.nl)
762 (Brinkman et al., 2014).
763
764 *VZV Flow Cytometry Infection Assay*
765
766 Cells were washed in FACS tubes with PBS and incubated with LIVE/DEAD Fixable
767 Violet Dead Cell Stain (Invitrogen) diluted 1:1000 in PBS for 30min at 4°C. Cells were
768 washed in PBS and resuspended in 100µl FACS buffer (1% FCS, 2mM EDTA in PBS)

769 containing 1:500 FITC-coupled antibody against VZV gE/gI complex. Cells were
770 incubated 30min at 4°C. After washing with PBS cells were resuspended in PBS and
771 an equal volume of 8% methanol-free formaldehyde in PBS was added. Cells were
772 fixed for 15min at room-temperature. Cells were washed with PBS, resuspended in
773 FACS buffer, and analysed on a Attune NxT Acoustic Focusing Cytometer (Thermo
774 Fisher).
775
776 *THP1 VZV Infections*
777
778 $6.125x10^6$ THP1 cells were seeded per well in 6-well plates in growth medium
779 containing 10 ng/ml PMA (Sigma-Aldrich). As a control, $1.625x10^6$ MeWo cells were
780 seeded in MEM. The next day cells were washed with PBS and overlaid with PBS
781 containing CellTrace Far Red dye (Invitrogen) diluted 1:5,000. Cells were labelled for
782 15min at 37°C, an excess of growth medium was added and cells were incubated for
783 another 5min. Meanwhile, aliquots of uninfected and VZV-infected MeWo cells were
784 thawed, washed, and resuspended in MEM. Cells were counted and their
785 concentration was adjusted to $6.25x10^5$ live cells per ml (for THP1 cells) or $1.25x10^5$
786 live cells per ml (for MeWo cells) with MEM. Medium was removed from labelled cells
787 and cells were overlaid with 2ml MeWo -/+VZV cell suspension. Cells were incubated
788 at 37°C for 1 hour. The cell suspension was removed, adherent cells were washed
789 with PBS, overlaid with their respective growth medium and incubated for 48 hours.
790 Supernatants were removed from cells, clarified by centrifugation and stored at -80°C.
791 CXCL10 levels were determined using Human CXCL10/IP-10 Quantikine ELISA Kit
792 (R&D Systems) according to manufacturer's instructions. Cells were washed with PBS
793 and incubated with Trypsin-EDTA until they started to detach. Growth medium was
794 added, cells were resuspended by gentle pipetting and transferred to FACS tubes on
795 ice. 45% of cell suspension were transferred to eppendorf tubes on ice for extraction
796 of RNA and generation of protein lysates, respectively. The cells in those eppendorf
797 tubes were pelleted, washed with PBS, and then lysed either in RLT buffer and
798 processed for RT-qPCR or lysed in RIPA buffer and processed for immunoblot
799 analysis. Remaining cells in FACS tubes were used for analysis by flow cytometry.
800
801 *Pulldowns*
802
803 $1.4x10^7$ HEK293T cells were seeded in 15cm cell culture dishes. The next day, cells
804 were transfected with 12.7µg of ORF9-V5, cGAS-FLAG, and STING-HA expression
805 plasmids using Lipofectamine 2000. 16 hours later, cells were lysed in IP buffer (20mM
806 TRIS-HCl pH7.4, 100mM NaCl, 1mM EDTA, 0.5% NP-40, Protease Inhibitor Cocktail
807 (CellSignaling Technology)). After clarification, an aliquot was removed as input
808 sample and the lysate was split into four equal volumes. Each aliquot was incubated
809 with 50µl Dynabeads Protein G that were coated with 5µg α-V5, α-FLAG, α-HA, or
810 control IgG antibody for 1 hour under rotation at 4°C. The supernatant was removed,
811 an aliquot was stored as unbound fraction from each sample, and beads were washed
812 three times in lysis buffer. Input, unbound, and bound fractions were subjected to
813 immunoblotting. For pulldowns from stably transduced THP1 cells, cells were seeded

814 at $2x10^7$ per dish in 15cm cell-culture dishes in growth medium containing 10ng/ml
815 PMA. Lysates were generated the next day and processed as described above. For
816 pulldowns of recombinant proteins, 3µl recombinant cGAS-HA protein was mixed with
817 1.5µl FLAG-ORF9 or FLAG-GFP in IP buffer. IP was performed as described above.
818 For pulldowns from VZV-infected cells, $2.2x10^7$ THP1 cells and $4x10^6$ HaCaT cells
819 were seeded in 10cm dishes (in the presence of 10ng/ml PMA for THP1 cells). The
820 next day cells were overlaid with $1.25x10^7$ MeWo cells infected with VZV or $VZV^{ORF9-}$
821 $^{V5}$ for 1 hour and afterwards washed with PBS. Lysates were generated 48 hours later
822 as described above.
823
824 *Far western*
825
826 The experimental procedure for far western was based on a protocol previously
827 described (Wu et al., 2007). 1.5µl FLAG-ORF9 protein or 1.5µl FLAG-GFP protein was
828 subjected to SDS-PAGE and blotting as described for regular immunoblotting (see
829 below). After transfer, the membrane was incubated for 30min at RT temperature in
830 AC buffer (6M Guanidine HCl, 100mM NaCl, 20mM TRIS-HCl pH 7.6, 0.5mM EDTA,
831 10% glycerol, 0.1% Tween-20, 2% skim milk powder, 1mM DTT). The membrane was
832 then incubated in AC buffers with decreasing concentrations of Guanidine HCl (3M,
833 1M, 0.1M) for 30min each. For the last incubation the membrane was transferred to
834 4°C and thereafter incubated in AC buffer free of Guanidine HCl overnight. The
835 membrane was blocked for 1 hour in 5% milk powder in PBST (PBS with 0.05%
836 Tween-20) and then incubated with 10µl recombinant cGAS per 5ml buffer as probe
837 in 3% milk powder in PBST for 1 hour. Membranes were washed for 10min with PBST
838 thrice and then incubated with α-cGAS antibody for 1 hour. After washing, membranes
839 were incubated with appropriate secondary antibodies, washed again, and imaged.
840 Hereafter, membranes were stripped and re-probed with α-FLAG antibody as
841 described for conventional immunoblot.
842
843 *Immunofluorescence*
844
845 $1.75x10^5$ HEK293T cells were seeded onto-glass coverslips. The next day, cells were
846 transfected with 250ng of cGAS-V5 or FLAG-ORF9 expression plasmid using 1.5µl
847 Lipofectamine 3000 per well. Additional coverslips were co-transfected with both
848 plasmids. 24 hours later cells were washed with PBS and fixed with 4% formaldehyde
849 in cytoskeleton stabilisation buffer (CSB; 10mM KCl, 274mM NaCl, 8mM $NaHCO_3$,
850 0.8mM $KH_2PO_4$, 2.2mM $Na_2HPO_4$, 4mM $MgCl_2$, 10mM PIPES, 4mM EGTA, 11mM
851 glucose) for 15min. Cells were washed and permeabilised with 0.1% Triton X-100 in
852 CSB for 20min and incubated with 100mM glycine in CSB for 10min afterwards. Cells
853 were washed with PBS four times and blocked using 1% BSA and 5% normal goat
854 serum (Invitrogen) in PBS for 1 hour. Coverslips were incubated with primary
855 antibodies in blocking solution for 3 hour at room temperature. Cells were washed
856 three times with PBS and incubated with secondary antibodies in blocking solution for
857 1 hour. Coverslips were washed with PBS three times and mounted onto glass slides

858 using ProLong Diamond Antifade Mountant with DAPI (Invitrogen). Images were
859 acquired using a Zeiss LSM780 confocal microscopy system (Zeiss).
860
861 *Recombinant Protein Expression*
862
863 BL21-pLysS-Rosetta *E.coli* (kind gift from Simon Davis, University of Oxford, UK) were
864 transformed with bacterial expression vectors. A single colony or a glycerol stock from
865 a single colony were used to inoculate a starter culture of 25ml LB-medium containing
866 34µg/ml Chloramphenicol and 100µg/ml Carbenicillin. A large 400ml LB culture was
867 inoculated using the starter culture. OD600 was measured in intervals and, for VZV
868 ORF9 and GFP, recombinant protein expression was induced by adding 0.1mM IPTG
869 once OD reached 0.6. Bacteria were grown 3 hours at 37°C. For expression of
870 recombinant cGAS and cGAS-HA, bacteria were grown to OD 0.8 and chilled to 18°C.
871 Protein expression was induced by adding 0.4mM IPTG and bacteria were incubated
872 for 16 hours at 18°C. For all proteins, bacteria were pelleted at 6,000g for 7min and
873 the pellet was resuspended in 12ml lysis buffer (20mM TRIS pH7.4, 500mM NaCl,
874 0.5mM EDTA, 0.5mM EGTA, 0.5% NP40, 1:100 Protease Inhibitor Cocktail
875 (CellSignaling Technology)). The suspension was sonicated on ice three times at 20%
876 amplitude with 15 sec ON and 30 sec OFF (Branson Sonifier). Insoluble material was
877 removed by centrifugation for 15min at 24,000g. In the meantime, 150µl Glutathione
878 Sepharose beads (GE Healthcare) were prepared according to manufacturer's
879 instructions. The beads were added to the clarified lysate and incubated under rotation
880 for 4 hours at 4°C. The beads were pelleted by centrifugation at 500g and washed five
881 times with lysis buffer. The beads were washed once in PreScission Cleavage buffer
882 (50mM TRIS pH 7.5, 150mM, 1mM freshly added DTT) and resuspended in 500µl
883 PreScission Cleavage buffer. After addition of 12µl PreScission Protease (GE
884 Healthcare), the suspension was incubated under rotation for 3 hours at 4°C. The
885 supernatant containing the recombinant protein was separated from beads and stored
886 at -80°C. Aliquots from the various purification steps were analysed by SDS-PAGE
887 and subsequent staining of the gel with EZBlue Gel Staining Reagent (Sigma Aldrich).
888 Based on band intensities the protein concentrations were estimated to be ca. 1µg/µl
889 for FLAG-ORF9 and FLAG-GFP, and ca. 0.5µg/µl for cGAS and cGAS-HA.
890
891 *Immunoblotting*
892
893 Protein concentrations in lysates were determined using Pierce BCA Protein Assay Kit
894 (Thermo Scientific) and equalised by dilution of samples with lysis buffer.
895 Subsequently, 4x NuPAGE LDS Sample Buffer (Invitrogen) was added and samples
896 were incubated at 95°C for 10min. Samples were run on NuPAGE Novex 4-12% Bis-
897 TRIS gels (Invitrogen) using NuPage MOPS-SDS running buffer (Invitrogen). Proteins
898 were subsequently blotted onto PROTRAN Pure nitrocellulose membrane
899 (PerkinElmer) using transfer buffer (25mM TRIS, 192mM glycine). Membranes were
900 blocked with 5% skim milk powder (Sigma-Aldrich) in TBS containing 0.1% Tween-20
901 (5% milk TBS-T) for 1 hour at room temperature and were then incubated with primary
902 antibodies in 5% milk TBS-T overnight at 4°C. Primary antibodies that bind to

903 phosphorylated residues were diluted in 5% BSA in TBS-T. Membranes were washed
904 thrice with TBS-T and incubated with HRP-coupled secondary antibodies in 5% milk
905 TBS-T for 1 hour at room temperature. After three further washes with TBS-T, proteins
906 were detected using Western Lightning Plus-ECL (PerkinElmer) and the iBright
907 FL1000 Imaging System (Thermo Fisher) or Amersham Hyperfilm MP (GE
908 Healthcare). If needed, antibodies were stripped from the membrane with stripping
909 buffer (200mM glycine, 0.1% SDS, 1% Tween-20, pH 2.2) for 20min at room
910 temperature. Membranes were washed with TBS-T, blocked as described above and
911 re-probed.
912
913 *RT-qPCR*
914
915 Cells were lysed in RLT Plus buffer and RNA was extracted using RNeasy Plus Mini
916 Kit (Qiagen). The RNA was reverse transcribed using SuperScript IV Reverse
917 Transcriptase (Invitrogen) and oligo-dT primers (Invitrogen). The qPCR reaction
918 containing TaqMan Universal PCR Master Mix (Applied Biosystems) and TaqMan
919 Primer/Probes was run on QuantStudio 7 Flex Real-Time PCR System (Thermo
920 Fisher) with standard settings. Gene expression was analysed with the Ct method
921 using *GAPDH* expression for normalisation. Taqman primer/probes used were:
922 *GAPDH* (Hs02758991_g1), *IFNB1* (Hs02621180_s1), *IFI44* (Hs00951349_m1), and
923 *IFNL1* (Hs00601677_g1).
924
925 *Protein sequence analysis*
926
927 The HSV-1 VP22 (PDB: 4XAL) and MHV68 ORF52 (PDB: 2OA5) crystal structures
928 were used to graphically represent secondary structure features. For VZV ORF9
929 (UniProt accession Q4JQW6) and KSHV ORF52 (UniProt accession F5HBL8),
930 structural features and sequence disorder was predicted by the PROFphd secondary
931 structure prediction algorithm through submission of protein sequences to the
932 predictprotein.org web interface (Yachdav et al., 2014).
933
934 *Data Analysis and Software*
935
936 Data were analysed using Excel for Mac (Microsoft) and GraphPad Prism 8 (GraphPad
937 Software). SnapGene (GSL Biotech) and ApE (M. Wayne Davis, The University of
938 Utah) were utilised for DNA sequence analysis to assist cloning. Statistical analysis is
939 detailed in the figure legends and was performed using GraphPad Prism 8. Graphs
940 and figures were created using GraphPad Prism 8 and Adobe Illustrator CC (Adobe
941 Systems). Immunoblot images were processed using web-based iBright Image
942 Analysis software (Thermo Fisher). Flow cytometry data was analysed using FlowJo
943 (FlowJo, LLC). Fiji 2.0.0 software was used to process confocal microscopy images
944 (Schindelin et al., 2012).
945

946 **REFERENCES**

947


948 Abendroth, A., Morrow, G., Cunningham, A.L., and Slobedman, B. (2001). Varicella-
949 zoster virus infection of human dendritic cells and transmission to T cells:
950 implications for virus dissemination in the host. J Virol *75*, 6183-6192.

951 Ablasser, A., and Chen, Z.J. (2019). cGAS in action: Expanding roles in immunity
952 and inflammation. Science *363*, eaat8657.

953 Ablasser, A., Goldeck, M., Cavlar, T., Deimling, T., Witte, G., Röhl, I., Hopfner, K.-P.,
954 Ludwig, J., and Hornung, V. (2013). cGAS produces a 2′-5′-linked cyclic dinucleotide
955 second messenger that activates STING. Nature *498*, 380-384.

956 Almine, J.F., O'Hare, C.A.J., Dunphy, G., Haga, I.R., Naik, R.J., Atrih, A., Connolly,
957 D.J., Taylor, J., Kelsall, I.R., Bowie, A.G.*, et al.* (2017). IFI16 and cGAS cooperate in
958 the activation of STING during DNA sensing in human keratinocytes. Nat Commun *8*,
959 679.

960 Andreeva, L., Hiller, B., Kostrewa, D., Lässig, C., de Oliveira Mann, C.C., Jan
961 Drexler, D., Maiser, A., Gaidt, M., Leonhardt, H., Hornung, V.*, et al.* (2017). cGAS
962 senses long and HMGB/TFAM-bound U-turn DNA by forming protein–DNA ladders.
963 Nature *549*, 394-398.

964 Arvin, A.M., and Gilden, D. (2013). Varicella-Zoster Virus. In Virology, B.N. Fields,
965 D.M. Knipe, and P.M. Howley, eds. (Philadelphia: Wolters Kluwer Health/Lippincott
966 Williams & Wilkins), pp. 2015-2057.

967 Arvin, A.M., Koropchak, C.M., Williams, B.R.G., Grumet, F.C., and Foung, S.K.H.
968 (1986). Early Immune Response in Healthy and Immunocompromised Subjects with
969 Primary Varicella-Zoster Virus Infection. The Journal of Infectious Diseases *154*, 422-
970 429.

971 Barrat, F.J., Elkon, K.B., and Fitzgerald, K.A. (2016). Importance of Nucleic Acid
972 Recognition in Inflammation and Autoimmunity. Annu Rev Med *67*, 323-336.

973 Bridgeman, A., Maelfait, J., Davenne, T., Partridge, T., Peng, Y., Mayer, A., Dong, T.,
974 Kaever, V., Borrow, P., and Rehwinkel, J. (2015). Viruses transfer the antiviral
975 second messenger cGAMP between cells. Science *349*, 1228-1232.

976 Brinkman, E.K., Chen, T., Amendola, M., and van Steensel, B. (2014). Easy
977 quantitative assessment of genome editing by sequence trace decomposition.
978 Nucleic Acids Res *42*, e168-e168.

979 Brito, A.F., and Pinney, J.W. (2018). Time-calibrated tree reconciliations reveal
980 frequent losses, intrahost speciations, and host switches in the evolution of
981 herpesviruses. Biorxiv, 418111.

982 Brubaker, S.W., Bonham, K.S., Zanoni, I., and Kagan, J.C. (2015). Innate immune
983 pattern recognition: a cell biological perspective. Annu Rev Immunol *33*, 257-290.

984 Buchan, D.W.A., and Jones, D.T. (2019). The PSIPRED Protein Analysis
985 Workbench: 20 years on. Nucleic Acids Res *47*, W402-W407.

986 Campbell, T.M., McSharry, B.P., Steain, M., Ashhurst, T.M., Slobedman, B., and
987 Abendroth, A. (2018). Varicella zoster virus productively infects human natural killer
988 cells and manipulates phenotype. PLoS Pathog *14*, e1006999.

989 Carter-Timofte, M.E., Paludan, S.R., and Mogensen, T.H. (2018). RNA Polymerase
990 III as a Gatekeeper to Prevent Severe VZV Infections. Trends in Molecular Medicine
991 *24*, 904-915.

992 Caunt, A.E., and Taylor-Robinson, D. (2009). Cell-free varicella-zoster virus in tissue
993 culture. Epidemiol Infect *62*, 413-424.

994 Chauveau, L., Bridgeman, A., Tan, T.K., Beveridge, R., Frost, J., Pedroza-Pacheco,
995 I., Partridge, T., Borrow, P., Drakesmith, H., Townsend, A.*, et al.* (2020). cGAMP
996 loading enhances the immunogenicity of VLP vaccines. Biorxiv,
997 2020.2001.2003.893586.

998 Che, X., Oliver, S.L., Reichelt, M., Sommer, M.H., Haas, J., Rovis, T.L., and Arvin,
999 A.M. (2013). ORF11 Protein Interacts with the ORF9 Essential Tegument Protein in
1000 Varicella-Zoster Virus Infection. J Virol *87*, 5106-5117.

1001 Che, X., Reichelt, M., Sommer, M.H., Rajamani, J., Zerboni, L., and Arvin, A.M.
1002 (2008). Functions of the ORF9-to-ORF12 Gene Cluster in Varicella-Zoster Virus
1003 Replication and in the Pathogenesis of Skin Infection. J Virol *82*, 5825-5834.

1004 Chen, J.J., Zhu, Z., Gershon, A.A., and Gershon, M.D. (2004). Mannose 6-
1005 Phosphate Receptor Dependence of Varicella Zoster Virus Infection In Vitro and in
1006 the Epidermis during Varicella and Zoster. Cell *119*, 915-926.

1007 Cohen, J.I., and Seidel, K.E. (1993). Generation of varicella-zoster virus (VZV) and
1008 viral mutants from cosmid DNAs: VZV thymidylate synthetase is not essential for
1009 replication in vitro. Proc Natl Acad Sci USA *90*, 7376-7380.

1010 Davison, A.J. (2002). Evolution of the herpesviruses. Vet Microbiol *86*, 69-88.

1011 de Oliveira Mann, C.C., Orzalli, M.H., King, D.S., Kagan, J.C., Lee, A.S.Y., and
1012 Kranzusch, P.J. (2019). Modular Architecture of the STING C-Terminal Tail Allows
1013 Interferon and NF-kappaB Signaling Adaptation. Cell Rep *27*, 1165-1175 e1165.

1014 Dempsey, A., and Bowie, A.G. (2015). Innate immune recognition of DNA: A recent
1015 history. Virology *479-480*, 146-152.

1016 Diner, E.J., Burdette, D.L., Wilson, S.C., Monroe, K.M., Kellenberger, C.A., Hyodo,
1017 M., Hayakawa, Y., Hammond, M.C., and Vance, R.E. (2013). The Innate Immune
1018 DNA Sensor cGAS Produces a Noncanonical Cyclic Dinucleotide that Activates
1019 Human STING. Cell Rep *3*, 1355-1361.

1020 Drayman, N., Patel, P., Vistain, L., and Tay, S. (2019). HSV-1 single-cell analysis
1021 reveals the activation of anti-viral and developmental programs in distinct sub-
1022 populations. Elife *8*, 2503.

1023 Du, M., and Chen, Z.J. (2018). DNA-induced liquid phase condensation of cGAS
1024 activates innate immune signaling. Science *361*, 704-709.

1025 Fitzgerald, K.A., McWhirter, S.M., Faia, K.L., Rowe, D.C., Latz, E., Golenbock, D.T.,
1026 Coyle, A.J., Liao, S.M., and Maniatis, T. (2003). IKKepsilon and TBK1 are essential
1027 components of the IRF3 signaling pathway. Nat Immunol *4*, 491-496.

1028 Freundt, E.C., Drappier, M., and Michiels, T. (2018). Innate Immune Detection of
1029 Cardioviruses and Viral Disruption of Interferon Signaling. Front Microbiol *9*, 867.

1030 Gerada, C., Campbell, T.M., Kennedy, J.J., McSharry, B.P., Steain, M., Slobedman,
1031 B., and Abendroth, A. (2020). Manipulation of the Innate Immune Response by
1032 Varicella Zoster Virus. Front Immunol *11*, 1.

1033 Haberthur, K., and Messaoudi, I. (2013). Animal Models of Varicella Zoster Virus
1034 Infection. Pathogens *2*, 364-382.

1035 Harding, S.M., Benci, J.L., Irianto, J., Discher, D.E., Minn, A.J., and Greenberg, R.A.
1036 (2017). Mitotic progression following DNA damage enables pattern recognition within
1037 micronuclei. Nature *548*, 466-470.

1038 Hartmann, G. (2017). Nucleic Acid Immunity. Adv Immunol *133*, 121-169.

1039 Hertzog, J., Dias Junior, A.G., Rigby, R.E., Donald, C.L., Mayer, A., Sezgin, E.,
1040 Song, C., Jin, B., Hublitz, P., Eggeling, C.*, et al.* (2018). Infection with a Brazilian
1041 isolate of Zika virus generates RIG-I stimulatory RNA and the viral NS5 protein
1042 blocks type I IFN induction and signaling. Eur J Immunol *48*, 1120-1136.

1043 Hew, K., Dahlroth, S.-L., Nordlund, P., Cornvik, T., and Pan, L.X. (2015). VP22 core
1044 domain from Herpes simplex virus 1 reveals a surprising structural conservation in
1045 both the Alpha- and Gammaherpesvirinae subfamilies. Journal of General Virology
1046 *96*, 1436-1445.

1047 Holm, C.K., Rahbek, S.H., Gad, H.H., Bak, R.O., Jakobsen, M.R., Jiang, Z., Hansen,
1048 A.L., Jensen, S.K., Sun, C., Thomsen, M.K.*, et al.* (2016). Influenza A virus targets a
1049 cGAS-independent STING pathway that controls enveloped RNA viruses. Nat
1050 Commun *7*, 10680.

1051 Horan, K.A., Hansen, K., Jakobsen, M.R., Holm, C.K., Soby, S., Unterholzner, L.,
1052 Thompson, M., West, J.A., Iversen, M.B., Rasmussen, S.B.*, et al.* (2013).
1053 Proteasomal degradation of herpes simplex virus capsids in macrophages releases
1054 DNA to the cytosol for recognition by DNA sensors. J Immunol *190*, 2311-2319.

1055 Hu, S., Sun, H., Yin, L., Li, J., Mei, S., Xu, F., Wu, C., Liu, X., Zhao, F., Zhang, D.*, et*
1056 *al.* (2019). PKR-dependent cytosolic cGAS foci are necessary for intracellular DNA
1057 sensing. Science Signaling *12*, eaav7934.

1058 Huang, J., You, H., Su, C., Li, Y., Chen, S., and Zheng, C. (2018). Herpes Simplex
1059 Virus 1 Tegument Protein VP22 Abrogates cGAS/STING-Mediated Antiviral Innate
1060 Immunity. J Virol *92*, 783.

1061 Ishikawa, H., Ma, Z., and Barber, G.N. (2009). STING regulates intracellular DNA-
1062 mediated, type I interferon-dependent innate immunity. Nature *461*, 788-792.

1063 Kennedy, J.J., Steain, M., Slobedman, B., and Abendroth, A. (2019). Infection and
1064 Functional Modulation of Human Monocytes and Macrophages by Varicella-Zoster
1065 Virus. J Virol *93*, 10980.

1066 Kim, J.-A., Park, S.-K., Seo, S.-w., Lee, C.H., and Shin, O.S. (2017). STING Is
1067 Involved in Antiviral Immune Response against VZV Infection via the Induction of
1068 Type I and III IFN Pathways. Journal of Investigative Dermatology *137*, 2101-2109.

1069 Kranzusch, P.J., Wilson, S.C., Lee, A.S.Y., Berger, J.M., Doudna, J.A., and Vance,
1070 R.E. (2015). Ancient Origin of cGAS-STING Reveals Mechanism of Universal 2′,3′
1071 cGAMP Signaling. Molecular Cell *59*, 891-903.

1072 Ku, C.-C., Chang, Y.-H., Chien, Y., and Lee, T.-L. (2016). Type I interferon inhibits
1073 varicella-zoster virus replication by interfering with the dynamic interaction between
1074 mediator and IE62 within replication compartments. Cell Biosci *6*, 519.

1075 Lebrun, M., Lambert, J., Riva, L., Thelen, N., Rambout, X., Blondeau, C., Thiry, M.,
1076 Snoeck, R., Twizere, J.-C., Dequiedt, F.*, et al.* (2018). Varicella-Zoster Virus ORF9p
1077 Binding to Cellular Adaptor Protein Complex 1 Is Important for Viral Infectivity. J Virol
1078 *92*, 222.

1079 Li, X., Shu, C., Yi, G., Chaton, C.T., Shelton, C.L., Diao, J., Zuo, X., Kao, C.C., Herr,
1080 A.B., and Li, P. (2013). Cyclic GMP-AMP Synthase Is Activated by Double-Stranded
1081 DNA-Induced Oligomerization. Immunity *39*, 1019-1031.

1082 Liu, S., Cai, X., Wu, J., Cong, Q., Chen, X., Li, T., Du, F., Ren, J., Wu, Y.T., Grishin,
1083 N.V.*, et al.* (2015). Phosphorylation of innate immune adaptor proteins MAVS,
1084 STING, and TRIF induces IRF3 activation. Science *347*, aaa2630.

1085 Luecke, S., Holleufer, A., Christensen, M.H., Jonsson, K.L., Boni, G.A., Sorensen,
1086 L.K., Johannsen, M., Jakobsen, M.R., Hartmann, R., and Paludan, S.R. (2017).
1087 cGAS is activated by DNA in a length-dependent manner. EMBO Rep *18*, 1707-
1088 1715.

1089 Lum, K.K., Song, B., Federspiel, J.D., Diner, B.A., Howard, T., and Cristea, I.M.
1090 (2018). Interactome and Proteome Dynamics Uncover Immune Modulatory
1091 Associations of the Pathogen Sensing Factor cGAS. Cell Syst *7*, 627-642.e626.

1092 Mackenzie, K.J., Carroll, P., Martin, C.-A., Murina, O., Fluteau, A., Simpson, D.J.,
1093 Olova, N., Sutcliffe, H., Rainger, J.K., Leitch, A.*, et al.* (2017). cGAS surveillance of
1094 micronuclei links genome instability to innate immunity. Nature *548*, 461-465.

1095 Mainka, C., Fuss, B., Geiger, H., Höfelmayr, H., and Wolff, M.H. (1998).
1096 Characterization of viremia at different stages of varicella-zoster virus infection. J
1097 Med Virol *56*, 91-98.

1098 McGeoch, D.J., Cook, S., Dolan, A., Jamieson, F.E., and Telford, E.A.R. (1995).
1099 Molecular Phylogeny and Evolutionary Timescale for the Family of Mammalian
1100 Herpesviruses. Journal of Molecular Biology *247*, 443-458.

1101 McNab, F., Mayer-Barber, K., Sher, A., Wack, A., and O'Garra, A. (2015). Type I
1102 interferons in infectious disease. Nat Rev Immunol *15*, 87-103.

1103 Mo, C., Lee, J., Sommer, M.H., and Arvin, A.M. (2003). Varicella-zoster virus
1104 infection facilitates VZV glycoprotein E trafficking to the membrane surface of
1105 melanoma cells. J Med Virol *70*, S56-S58.

1106 Morrow, G., Slobedman, B., Cunningham, A.L., and Abendroth, A. (2003). Varicella-
1107 Zoster Virus Productively Infects Mature Dendritic Cells and Alters Their Immune
1108 Function. J Virol *77*, 4950-4959.

1109 Nagel, M.A., and Gilden, D. (2014). Neurological complications of varicella zoster
1110 virus reactivation. Current Opinion in Neurology *27*, 356-360.

1111 Nour, A.M., Reichelt, M., Ku, C.-C., Ho, M.Y., Heineman, T.C., and Arvin, A.M.
1112 (2011). Varicella-Zoster Virus Infection Triggers Formation of an Interleukin-1β (IL-
1113 1β)-processing Inflammasome Complex. J Biol Chem *286*, 17921-17933.

1114 Radtke, K., Döhner, K., and Sodeik, B. (2006). Viral interactions with the
1115 cytoskeleton: a hitchhiker's guide to the cell. Cell Microbiol *8*, 387-400.

1116 Rehwinkel, J., Tan, C.P., Goubau, D., Schulz, O., Pichlmair, A., Bier, K., Robb, N.,
1117 Vreede, F., Barclay, W., Fodor, E.*, et al.* (2010). RIG-I Detects Viral Genomic RNA
1118 during Negative-Strand RNA Virus Infection. Cell *140*, 397-408.

1119 Riva, L., Thiry, M., Bontems, S., Joris, A., Piette, J., Lebrun, M., and Sadzot-Delvaux,
1120 C. (2013). ORF9p Phosphorylation by ORF47p Is Crucial for the Formation and
1121 Egress of Varicella-Zoster Virus Viral Particles. J Virol *87*, 2868-2881.

1122 Riva, L., Thiry, M., Lebrun, M., L'Homme, L., Piette, J., and Sadzot-Delvaux, C.
1123 (2015). Deletion of the ORF9p Acidic Cluster Impairs the Nuclear Egress of Varicella-
1124 Zoster Virus Capsids. J Virol *89*, 2436-2441.

1125 Schindelin, J., Arganda-Carreras, I., Frise, E., Kaynig, V., Longair, M., Pietzsch, T.,
1126 Preibisch, S., Rueden, C., Saalfeld, S., Schmid, B.*, et al.* (2012). Fiji: an open-source
1127 platform for biological-image analysis. Nat Methods *9*, 676-682.

1128 Schoggins, J.W. (2019). Interferon-Stimulated Genes: What Do They All Do? Annu
1129 Rev Virol *6*, 567-584.

1130 Schoggins, J.W., Wilson, S.J., Panis, M., Murphy, M.Y., Jones, C.T., Bieniasz, P.,
1131 and Rice, C.M. (2011). A diverse range of gene products are effectors of the type I
1132 interferon antiviral response. Nature *472*, 481-485.

1133 Sen, N., Sommer, M., Che, X., White, K., Ruyechan, W.T., and Arvin, A.M. (2010).
1134 Varicella-Zoster Virus Immediate-Early Protein 62 Blocks Interferon Regulatory
1135 Factor 3 (IRF3) Phosphorylation at Key Serine Residues: a Novel Mechanism of
1136 IRF3 Inhibition among Herpesviruses. J Virol *84*, 9240-9253.

1137 Shakya, A.K., O'Callaghan, D.J., and Kim, S.K. (2019). Interferon Gamma Inhibits
1138 Varicella-Zoster Virus Replication in a Cell Line-Dependent Manner. J Virol *93*, 3904.

1139 Sharma, S., tenOever, B.R., Grandvaux, N., Zhou, G.P., Lin, R., and Hiscott, J.
1140 (2003). Triggering the interferon antiviral response through an IKK-related pathway.
1141 Science *300*, 1148-1151.

1142 Smith, G.L., Talbot-Cooper, C., and Lu, Y. (2018). Chapter Fourteen - How Does
1143 Vaccinia Virus Interfere With Interferon? In Advances in Virus Research, M. Kielian,
1144 T.C. Mettenleiter, and M.J. Roossinck, eds. (Academic Press), pp. 355-378.

1145 Stempel, M., Chan, B., and Brinkmann, M.M. (2019). Coevolution pays off:
1146 Herpesviruses have the license to escape the DNA sensing pathway. Med Microbiol
1147 Immunol *208*, 495-512.

1148 Sun, L., Wu, J., Du, F., Chen, X., and Chen, Z.J. (2013). Cyclic GMP-AMP Synthase
1149 Is a Cytosolic DNA Sensor That Activates the Type I Interferon Pathway. Science
1150 *339*, 786-791.

1151 Tischer, B.K., Kaufer, B.B., Sommer, M., Wussow, F., Arvin, A.M., and Osterrieder,
1152 N. (2007). A Self-Excisable Infectious Bacterial Artificial Chromosome Clone of
1153 Varicella-Zoster Virus Allows Analysis of the Essential Tegument Protein Encoded by
1154 ORF9. J Virol *81*, 13200-13208.

1155 Torigo, S., Ihara, T., and Kamiya, H. (2000). IL-12, IFN-gamma, and TNF-alpha
1156 released from mononuclear cells inhibit the spread of varicella-zoster virus at an
1157 early stage of varicella. Microbiol Immunol *44*, 1027-1031.

1158 Uetz, P., Dong, Y.-A., Zeretzke, C., Atzler, C., Baiker, A., Berger, B., Rajagopala,
1159 S.V., Roupelieva, M., Rose, D., Fossum, E.*, et al.* (2006). Herpesviral Protein
1160 Networks and Their Interaction with the Human Proteome. Science *311*, 239.

1161 Unterholzner, L., Keating, S.E., Baran, M., Horan, K.A., Jensen, S.B., Sharma, S.,
1162 Sirois, C.M., Jin, T., Latz, E., Xiao, T.S.*, et al.* (2010). IFI16 is an innate immune
1163 sensor for intracellular DNA. Nat Immunol *11*, 997-1004.

1164 Wang, J.P., Kurt-Jones, E.A., Shin, O.S., Manchak, M.D., Levin, M.J., and Finberg,
1165 R.W. (2005). Varicella-Zoster Virus Activates Inflammatory Cytokines in Human
1166 Monocytes and Macrophages via Toll-Like Receptor 2. J Virol *79*, 12658-12666.

1167 West, A.P., Khoury-Hanold, W., Staron, M., Tal, M.C., Pineda, C.M., Lang, S.M.,
1168 Bestwick, M., Duguay, B.A., Raimundo, N., MacDuff, D.A.*, et al.* (2015).
1169 Mitochondrial DNA stress primes the antiviral innate immune response. Nature *520*,
1170 553-557.

1171 WHO (2014). Varicella and herpes zoster vaccines: WHO position paper, June 2014.
1172 Weekly epidemiological record *25*, 265-288.

1173 Wu, J., Sun, L., Chen, X., Du, F., Shi, H., Chen, C., and Chen, Z.J. (2013). Cyclic
1174 GMP-AMP Is an Endogenous Second Messenger in Innate Immune Signaling by
1175 Cytosolic DNA. Science *339*, 826.

1176 Wu, J.J., Li, W., Shao, Y., Avey, D., Fu, B., Gillen, J., Hand, T., Ma, S., Liu, X., Miley,
1177 W.*, et al.* (2015). Inhibition of cGAS DNA Sensing by a Herpesvirus Virion Protein.
1178 Cell Host Microbe *18*, 333-344.

1179 Wu, Y., Li, Q., and Chen, X.-Z. (2007). Detecting protein–protein interactions by far
1180 western blotting. Nat Protoc *2*, 3278-3284.

1181 Yachdav, G., Kloppmann, E., Kajan, L., Hecht, M., Goldberg, T., Hamp, T.,
1182 Honigschmid, P., Schafferhans, A., Roos, M., Bernhofer, M.*, et al.* (2014).
1183 PredictProtein-an open resource for online prediction of protein structural and
1184 functional features. Nucleic Acids Research *42*, W337-W343.

1185 Yoneyama, M., Kikuchi, M., Natsukawa, T., Shinobu, N., Imaizumi, T., Miyagishi, M.,
1186 Taira, K., Akira, S., and Fujita, T. (2004). The RNA helicase RIG-I has an essential
1187 function in double-stranded RNA-induced innate antiviral responses. Nat Immunol *5*,
1188 730-737.

1189 Yu, H.-R., Huang, H.-C., Kuo, H.-C., Sheen, J.-M., Ou, C.-Y., Hsu, T.-Y., and Yang,
1190 K.D. (2011). IFN-α production by human mononuclear cells infected with varicella-
1191 zoster virus through TLR9-dependent and -independent pathways. Cell Mol Immunol
1192 *8*, 181-188.

1193 Zerboni, L., Sen, N., Oliver, S.L., and Arvin, A.M. (2014). Molecular mechanisms of
1194 varicella zoster virus pathogenesis. Nat Rev Microbiol *12*, 197-210.

1195 Zhang, C., Shang, G., Gui, X., Zhang, X., Bai, X.-c., and Chen, Z.J. (2019). Structural
1196 basis of STING binding with and phosphorylation by TBK1. Nature *567*, 394-398.

1197 Zhang, X., Shi, H., Wu, J., Zhang, X., Sun, L., Chen, C., and Chen, Z.J. (2013).
1198 Cyclic GMP-AMP Containing Mixed Phosphodiester Linkages Is An Endogenous
1199 High-Affinity Ligand for STING. Molecular Cell *51*, 226-235.

1200 Zhang, X., Wu, J., Du, F., Xu, H., Sun, L., Chen, Z., Brautigam, C.A., Zhang, X., and
1201 Chen, Z.J. (2014). The Cytosolic DNA Sensor cGAS Forms an Oligomeric Complex
1202 with DNA and Undergoes Switch-like Conformational Changes in the Activation
1203 Loop. Cell Rep *6*, 421-430.

1204 Zhou, W., Whiteley, A.T., de Oliveira Mann, C.C., Morehouse, B.R., Nowak, R.P.,
1205 Fischer, E.S., Gray, N.S., Mekalanos, J.J., and Kranzusch, P.J. (2018). Structure of
1206 the Human cGAS–DNA Complex Reveals Enhanced Control of Immune
1207 Surveillance. Cell *174*, 300-311.e311.

1208 Zhu, H., Zheng, C., Xing, J., Wang, S., Li, S., Lin, R., and Mossman, K.L. (2011).
1209 Varicella-Zoster Virus Immediate-Early Protein ORF61 Abrogates the IRF3-Mediated
1210 Innate Immune Response through Degradation of Activated IRF3. J Virol *85*, 11079-
1211 11089.
1212